POLITECNICO DI TORINO

Facoltà di Ingegneria
Corso di Laurea in Nanotecnologies for ICTs

Tesi di Laurea

Study and developement of new materials for harvest energy from CO_2 emissions

Relatore:
Andrea Lamberti

Candidato:
Davide Molino

Luglio 2020

Table of contents

Summary

Nowadays, Earth is undergoing effects of climate change due to the exponential increase of greenhouse gasses's emissions. The main component of greenhouse emissions is carbon dioxide (CO_2), which is estimated responsible for about 60% of global warming generated by human activities, and its concentration is increased by 40% [1] with respect to the concentration at the beginnings of industrial era.
This increase is due to several factors such as the combustion of coal, oil and gas and the progressive deforestation: this last phenomenon generates a sort of bottleneck in the so called biogeochemical "carbon cycle". Deforestation causes the lack of one of the natural regulating sources of carbon dioxide concentration.
Scientists set an increase of $2°C$ [1] (with respect to the pre-industrial global temperature) as the threshold beyond which there is a much higher risk that dangerous and possibly catastrophic changes in the global environment will occur. Nowadays the increase of the temperature has reached about $+0{,}85°C$ [1] thanks to greenhouse gasses. All technologies developed in CO_2 capturing have to be intended in the reduction of global warming.
In this thesis the goal is to develop a device able to harvest energy from carbon dioxide harvesting, exploiting graphene based super-capacitors and both aqueous solutions and ionic liquids as electrolytes. The intent of the device is to cutting down greenhouse emissions by reusing human produced carbon dioxide. Strategy to apply is capacitive mixing, which was a concept firstly applied to energy harvesting from salinity gradients: flowing through a capacitor (in which electrodes are modified using ion exchange membranes) alternatively salty water and fresh water, we modify the electrical double layer at the electrode-electrolyte interface. Ion exchange membranes allow the selective accumulation of opposite sign ions on the opposite electrodes. In this way it is possible to generate a DC power. Since there is no technology able to harvest mixing energy from gas sources, the idea was to adapt capmix in order to do so: we alternatively flush inside the electrolyte in an ion exchange membrane modified super-capacitor firstly CO2, then N2. In this way we have no more a salinity gradient, but a gradient in CO2 concentration. The idea is to exploit the conducibility reaction linked to adsorption carbon dioxide in a certain electrolyte in order to harvest energy in a similar way to one developed in capacitive mixing.

Chapter 1

State of the art

The ideas of harvest energy from CO_2 emissions were rosen from the experiments made on the harvesting from the gradient of salinity between sea water and river water (which is called blue energy) [2, 3]. In particular Blue energy is based on the harvest of mixing energy: when we mix (in irreversible way) 2 solutions with different concentrations and different volumes, we generate a Gibbs free energy which is equal to the difference between the final and the initial state [4]. The obtained energy is strictly related to the increase of entropy of the entire system and, if the mix is handled in an appropriate way, we are able to extract energy.
In this chapter we firstly discuss the techniques adopted in this field, and then we will move to the analysis of possible techniques we can adopt in order to capture carbon dioxide and produce energy.
We have generally 3 different types of approaches that exploit different phenomena, but all based on the use of membranes [2]: pressure retarded osmosis (PRO) [5], reverse electrodialysis (RED) [6] and membrane assisted capacitive mixing [7].

1.1 Pressure retarded osmosis

This kind of process is based on the osmosis phenomenon (the natural diffusion of a solvent from a less concentrated solution to a more concentrated one) and takes inspiration from desalination of sea water techniques [2]. In this technique it is fundamental the presence of a semipermeable membrane which allows only the flow of water and blocks the diffusion of any other particle [5].
Since the technique is based on 2 solutions with different concentration of solute, one of the places in which we have combination of different concentrated water based solutions is at river mouths, and so exploit the osmosis phenomenon that takes place between fresh water and salty water.
In figure 1.1 it is possible to observe the general setup adopted for pressure retarded

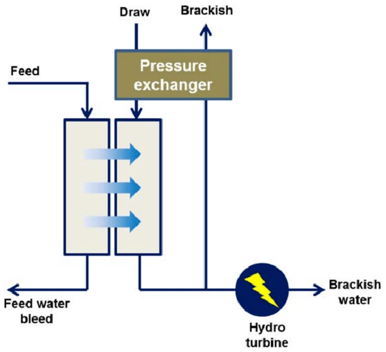

Figure 1.1: Schematic of a PRO process [5]

osmosis: the key element of the structure is an exchange cell, divided in 2 by the presence of a semipermeable membrane. The idea is to fill both semi-cells with the 2 solutions we have (salty and fresh water). The membrane, due to osmosis, will let flow water from the fresh water side to the salty water side, in order to try to balance the concentration we have on different sides of the membrane. In this way osmosis will generate a pressure increase on the salty water side, which is used to activate an hydro turbine which produces energy. In order to keep constant the pressure needed to spin the turbine, the system must be maintained in out of equilibrium conditions, which means ensure a constant feed of water on both sides and maintain stable the gradient of salt concentration between fresh water and sea water. It has to be noticed that the kind of potential exploited here to produce energy is a mechanical potential [5].

The principal issues of this technique are related to the type of membrane and to the water feed system. The membrane has to be selected in order to guarantee good permeability to water, able to stop the diffusion of salt and with the capability to work for very long times [5]. The issue related to the water feed system is due to the energy needed by the pumping apparatus in order to work correctly: this will necessarily reduce in a consistent way the available amount of energy produced (valued in 25% of the total power production [2]).

One of the first implants that uses this technology was opened in 2009 in Tofte, Norway, by Statkraft (one of the largest European companies in renewable sources). The plant was able to run at 10kW capacity with an initial membrane energy density of 1 W/m^2. However in order to make the production economically competitive, it is required a power production of 5 W/m^2. In 2014 the company decided to stop investments because of the lack of efficient and cheap membranes suitable for this application [8].

1.2 Reverse electrodyalisis

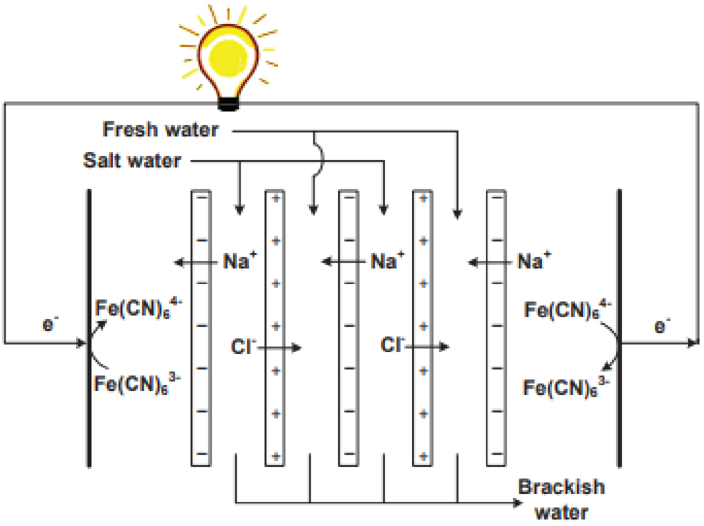

Figure 1.2: Schematic of a RED process [6]

As the previous case, also this technique takes inspiration on a desalination technique: in particular it is based on the electrodialysis. Both RED and ED exploit the same setup depicted in figure 1.2 [6]. The first technique is used in order to produce energy, the second one is intended to obtain pure water from sea water. In the electrodialysis a voltage is applied to the salty water inducing through this the collection of the cations and anions of the salt into a unique solution of brakish water [2]. Ionic exchange membranes are used to confine ions and prevent their redistribution in the dissalted water.

In this case, we exploit directly charges already present in the sea water. To do so, we exploit the setup shown in figure 1.2, which substantially is constituted by two external electrodes among which are placed several stacks of membranes, which are the elements that actually generate the voltage thanks to their ability to attract selectively cations or anions coming from the Donnan potential: this kind of membranes are characterized by a surface charge able to attract one kind of charge and reject the opposite, as explained in section 2.4 [?]. The outer electrodes are contacted to the first internal membranes by means of a redox solution (typically ferrocyanide-ferricyanide redox couples), in order to turn the ionic transport mechanism into an electronic one. Deeper in the device, we have several stacks of membranes: we will consider a single stack. Each stack is composed by 2 compartments (one devoted to fresh water, the other to salty water) and 2 exchange membranes (that contact the closest compartments) [6]. The alternation of anion exchange membrane and cation exchange membrane, together with the alternation of high

and low concentration solutions flowing in each compartment, allows to capture the mixing energy of the fresh water with the sea water. This kind of energy is related to the increase of entropy we observe each time we mix together 2 solutions without inducing chemical reactions. Because of the increase of entropy, we experience a release of energy, which can be collected and converted into a power source. The spontaneous movement of ions due to the attraction of membranes (Donnan potential, at section 2.4), induces a current in the external circuit, producing power. Each stack produces a voltage equal to 0,1 − 0,2 V, gathering several of them is possible to increase the total obtained voltage [6].
The main issues are due to the high cost of the exchange membranes, however the increase of the global demand can lower the total price. This technique, as the PRO, provides a DC power [6, 2].

1.3 Membrane assisted capacitive mixing

The device's setup is similar to a single stack of the RED setup, but in this case it is capacitor-based: in order to increase as much as possible the capacitance, generally are exploited carbon based super-capacitors, which are able to store more charges with respect standard capacitors. This is needed to increase as much as possible the amount of harvested energy. These techniques can be exploited only using electrical double layer capacitors (EDLC) and not super-capacitors in general. Moreover electrolyte has to be free to move, in order to allow the correct mixing between 2 different electrolytes we want to mix.

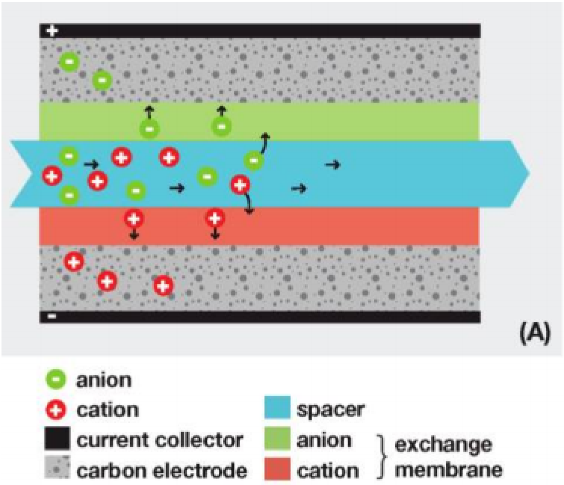

Figure 1.3: Setup of a device that harvest energy from capmix [7]

The origin of this renewable source of energy stands on the entropy increase we

observe when we mix 2 solutions with different salt concentration. This entropy increase can be handled in order to generate electrical energy.
In this technique, we flow alternatively salty and fresh water inside the device. In this way we modify the electrical double layer at the supercapacitor interfaces: when we have saline water inside the device, thanks to the exchange membranes, we have accumulation of anions on one electrode and cations on the opposite one [7, 9]. When we replace the salty water with fresh water, the entire system becomes unbalanced, because of the release of ions from the membranes. When we have open circuit conditions, the accumulation of ions on the anode and cathode produce only a voltage swing, so no power consumption. When we connect anode and cathode together by means of a resistance, we let flow through the resistance itself a current that follows the swing of the voltage, thus the generated power is a DC power [9]. We need to pay attention on the value selection of the resistance: the resistance has to guarantee the maximum possible power, but also to avoid losses due to internal resistances. The higher is the resistance, the lower are the generated power and losses, the lower is the resistance, the higher are generated power and internal losses. Generally the value adopted for the resistance is around 5 *Ω* and 30 *Ω* [9].

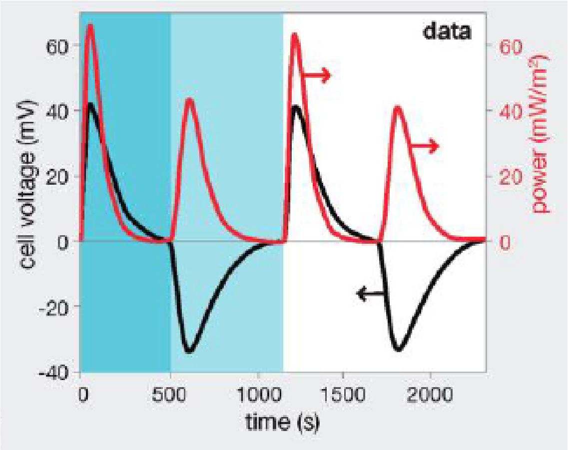

Figure 1.4: Shape of voltage and power during membrane assisted capacitive mixing process [7]

The obtained shape of voltage and power is depicted in figure 1.4: each time we change the type of electrolyte, we have a sharp change in voltage, and so in power production. The change is positive when we flow saline water, since in this situation we are charging the capacitors by means of membranes which are capturing ions. When we instead flow fresh water, we have a negative peak, since in this section of the process we are discharging the EDLC (membranes release the captured ions of the previous step) [9]. Here the energetic gain is due to the fact that once flushed the water inside the device, the power is spontaneously produced by the motion of ions inside the solution.

1.4 Harvesting from CO_2 exploiting mixing energy

The adopted technique is based on the same principle of membrane assisted capacitive mixing used in blue energy harvesting [9, 7], presented in previous section 1.3. However in this case we have to deal with energy coming from mix of gas source. The goal is to find a way to exploit also this kind of energy: to do so, we exploit a similar setup to the previous case (figure 1.8) [3]. Here we have a device composed by basically 2 sections. The core part of the setup is a carbon based EDL supercapacitor with plates modified with ionic exchange membranes, as in the case of membrane assisted capacitive mixing for blue energy harvesting. Then we have a pre-treatment section of the electrolyte, which is a water based solution: in 2 separate chambers, we flush the gas inside the electrolyte(this process is called gas sparging) [3]. One of these chambers is devoted to CO_2 sparging, the other one is devoted to air sparging.

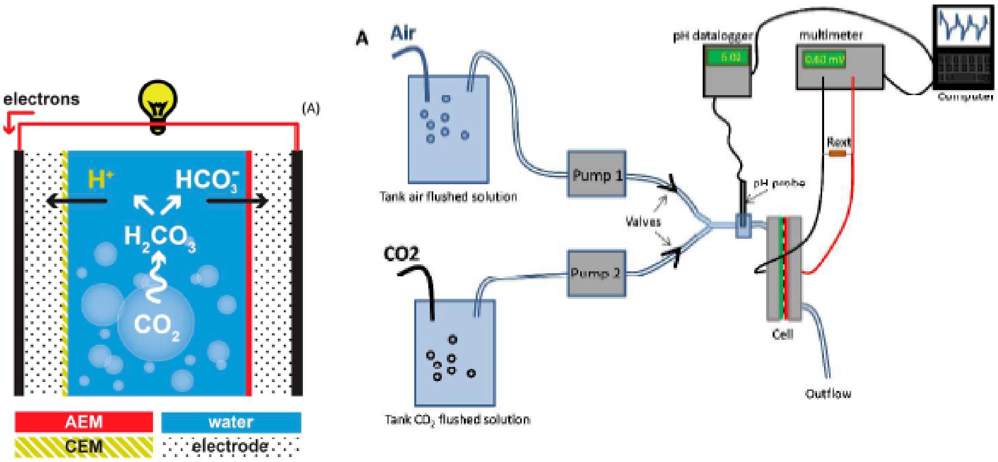

Figure 1.5: Setup of CO_2 harvesting technique [3]

When we sparge gas inside the electrolyte, we induce a chemical absorption of carbon dioxide [3]:

$$H_2O + CO_2 \longrightarrow H_2CO_3 \longleftrightarrow H^+ + HCO_3^- \tag{1.1}$$

The difference in the concentration of CO_2 in the sparging generates in the electrolytes a distinct concentration of carbonic acid in the 2 electrolytes. This will cause a difference in the ion concentration between the solutions, which can be exploited in order to harvest energy, flowing alternatively the treated electrolytes inside the EDL super-capacitor. The mechanisms that take place inside the device are the same we already analyzed previous in section 1.3 [3, 7, 9].

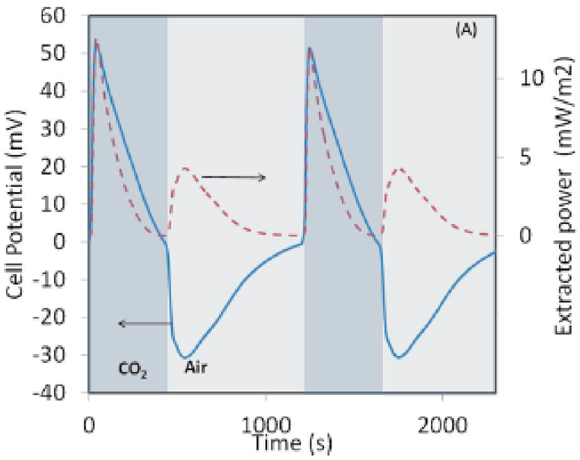

Figure 1.6: Voltage with respect time [3]

The main issue regarding this technique is due to the low efficiency of the flushing process: the energy produced is lower than the energy needed in order to correctly flush gas inside the electrolyte [3]. In order to make this process favourable, the idea is to increase the absorption of CO_2 by the electrolyte and so select in an appropriate way the correct electrolyte.

1.5 Harvesting from CO_2 exploiting pH gradient

In this case the idea is slightly different: we do not alternatively flush inside the EDL super-cap 2 electrolytes treated in different ways, but we have inside the device a both at the same time both the electrolytes, thanks to the different setup adopted (figure 1.7).

The setup is composed by 2 separate chambers in which is performed the sparging process: in the left chamber (referring to figure 1.7) we sparge with pure CO_2, while in the right chamber we sparge the electrolyte with air. The electrolyte is water based. Both chambers are connected directly with a cell made up by 2 MnO_2 electrodes. The cell is halved by a non selective membrane that allows the contact between the CO_2 sparged and the air sparged electrolyte. Inside the electrolyte we produce again the same reaction observed in the previous case (formula 1.1). Exploiting pH gradient across the membrane, we are able to avoid the use of ion

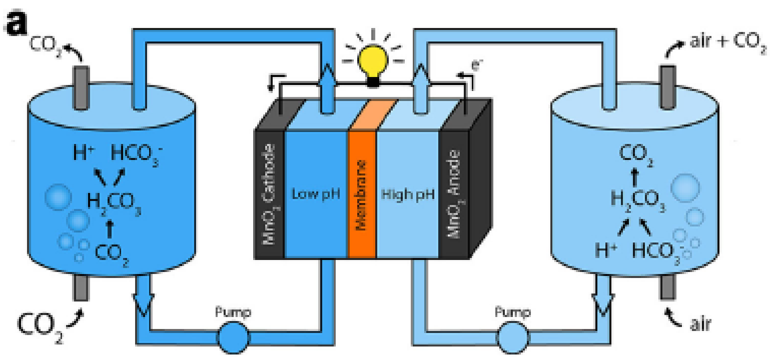

Figure 1.7: Setup of CO_2 harvesting technique [10]

selective membranes, using a cheaper non selective one [10].
The presence of CO_2 in water generates a basic ambient. However the concentration of CO_2 is different in the 2 pretreated electrolytes, so also the total pH is different depending on the concentration of carbon dioxide and this gives rise to a potential differences across the membrane. The electrolytes are treated in order to be able to conduct electricity (generally a 1M solution with a salt is adopted) and alternately fluxed both electrolytes in the 2 semi-cells [10]. This alternation generates a reversion of voltage at each change of flux, developing a pseudoequilibrium cell voltage. The obtained power density and cell voltage trend is very close to the trends obtained with capacitive mixing. Connecting electrodes with a resistance, we induce an alternate current. Considerations made in section 1.3 regarding the choose of the correct value for the resistance.

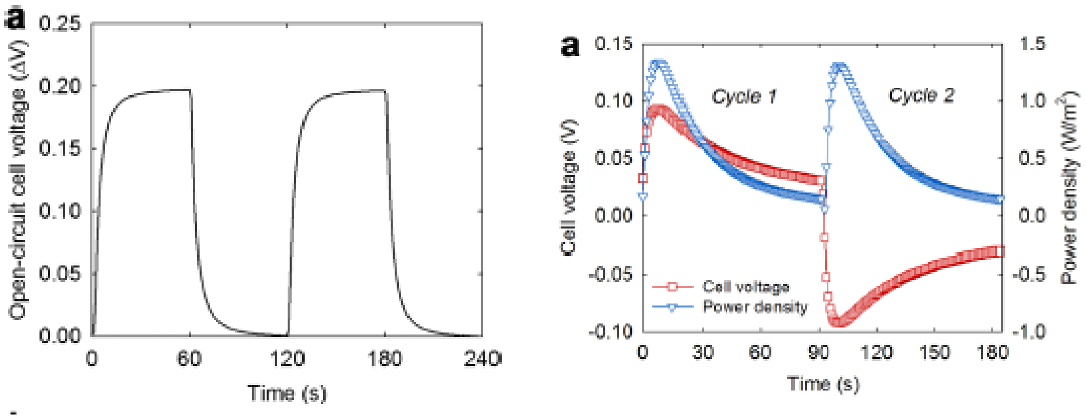

Figure 1.8: On the left the voltage swing with an open circuit measurement, on the right the behaviour of voltage, when the electrodes are connected together through a resistance [10]

Chapter 2

Device components

In this chapter we will analyze singularly each part that constitutes the capacitive device, meaning an overview on the working mechanism of super-capacitor, how work the membranes and how the electrolyte selected can affect the performances of the device. As already mentioned, we want to exploit a membrane modified flowing electrical double layer capacitor (EDLC), since we want to be able to change the electrolyte inside the super-cap. It has to be noticed how the membrane modification is widely studied in the case of capacitive mixing based on Donnan potential, while this modification inside an EDLC is an innovative concept.

2.1 Super-capacitor

A capacitor is a passive electric element able to store energy, usually through an electrostatic field or exploiting electrochemical processes [11]. Its structure is composed by 2 electrodes immersed in an electrolyte solution that acts as dielectric and a separator used to prevent short circuits between the electrodes.

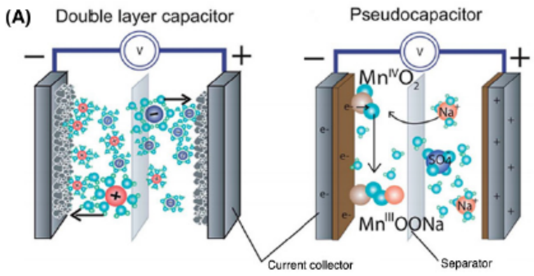

Figure 2.1: Typical structure of 2 types of super-capacitors: EDLC on the left and pseudo-capacitor on the right [12]

The charge happens through the application of a potential difference between the electrodes and once the capacitor is charged it can act like a power source when connected to an electrical circuit. The ability to store energy at a setted voltage is the capacitance and it is defined as the ratio between the stored charge and the potential difference applied to store it [11]:

$$C = \frac{Q}{V} \tag{2.1}$$

Another way to define the capacitance is through the construction characteristics of the device [11]:

$$C = \frac{\epsilon_0 \epsilon_r A}{D} \tag{2.2}$$

In this second equation, it is evident we can modify the capacitance of the device acting on 3 different parameters: the active area of the plates (A), the distance between the electrodes (D) and the type of electrolyte (ϵ_r). Since the way we want to exploit to harvest energy deals with the storage of charged particles, we need a device with the higher possible capacitance. In particular carbon based electrodes are a good choice to obtain an high capacitance because of their high specific area (1000-3000 m^2/g [11]).
With the Ragone plot, we are able to compare different type of power supply systems: in the following are reported fuel cells, batteries, electrochemical capacitors and standard capacitors.

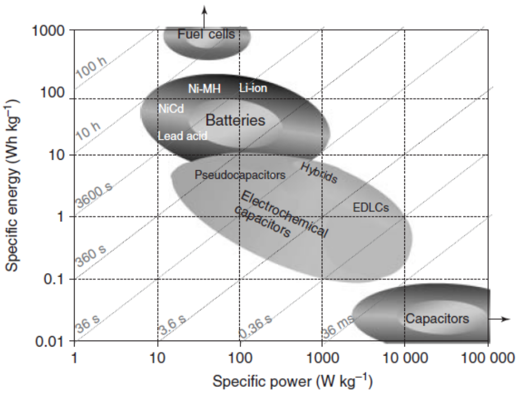

Figure 2.2: Ragone plot: specific power vs specific energy [11]

The Ragone plot is a figure of merit proposed by Ragone in 1968, with a view to find a good alternative to internal combustion engine in the automotive sector: this plot gives a comparison of performances for different energy sources and their effective yield. His purpose was to relate ”battery characteristics [which were the selected alternative supply] and the automotive power source requirements and to review the status of various traction battery systems" [13]. Nowadays this type of plot is still adopted to compare performances of charge storing devices. The analyzed physical dimensions are energy and power delivered. These are defined as follows [11]:

$$E = \frac{1}{2}CV^2 \tag{2.3}$$

$$P = \frac{E}{t} \quad , \quad P_{MAX} = \frac{V^2}{4ESR} \tag{2.4}$$

The power is defined as the energy delivered in a certain interval of time, but we have to notice that this power is limited by the internal resistance of the capacitor: equivalent series resistance (ESR), which takes into account all the resistive contributions due to internal components. This introduces a voltage drop and determines the maximum voltage of the capacitor during discharge and therefore limits the maximum energy and power of a capacitor. Generally either energy and power are normalized: in case of super-capacitors the normalization is with respect to the electrodes weight, since it is not always trivial to define the active area of a super-capacitor [11].
As figure 2.2 shows, super-capacitors are referred to as electrochemical capacitors (EC) in order to represent the fact that during charging/discharging processes are involved both Faradic and non Faradic reactions. In the following picture are represented in a tree scheme all classes of capacitors.

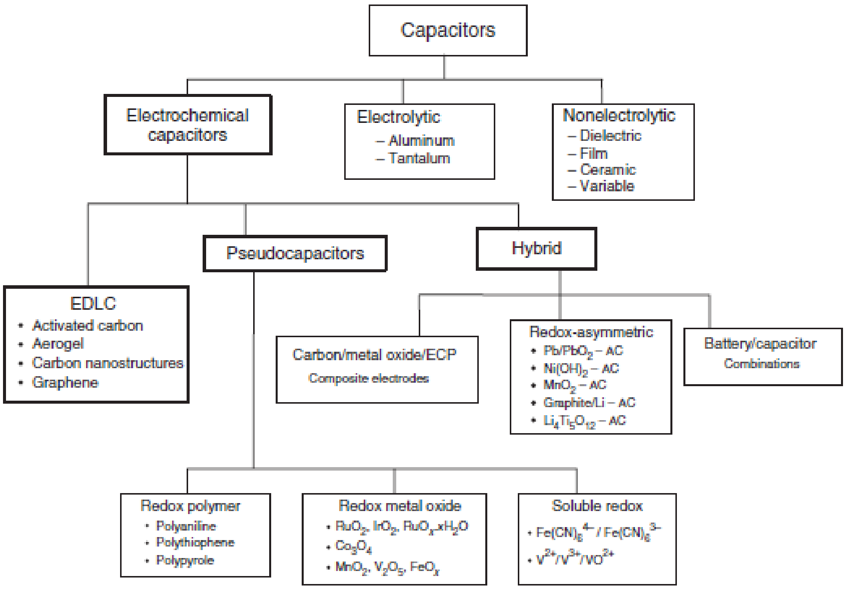

Figure 2.3: Different kind of capacitors and storing mechanism [11]

Here in this thesis we will focus on Electrical double layer capacitors based on activated carbons. However can be useful to analyze also others mechanisms of charge storage in EC capacitors. The 3 different branches are:

- Electrical double layer: the working principle is based on the formation of Helmoltz layers at the electrode-electrolyte interface on both electrodes, so is a non-Faradic process. The resulting capacitance of the entire device is the combination of the semi-capacitances generated on both electrodes. These have to guarantee the higher possible area in order to maximize the capacitance: this result can be achieved exploiting high effective area materials or engineering geometries of the device. Activated carbon, due to its high porosity, is a suitable material to exploit this phenomenon.

- Pseudo-capacitance: this type of devices are based on fast and reversible redox reactions, which are Faradic processes. This type of capacitance is not an electrostatic one, but occurs when we observe a charge transfer between electrolyte and electrode. Materials used as electrodes for this kind of technique are metal oxides and conductive polymers.

- Hybrid: in this kind of super-capacitors both Faradic and non-Faradic processes are involved in the generation of the capacitance.

Coming back to Ragone plot (figure 2.2), we can notice that super-capacitors can guarantee higher power density with respect to batteries and higher density of energy than standard capacitors: this means that they can store more energy than a standard capacitor and are able to charge and discharge faster than a battery. Moreover they have a long life cycle, compared to batteries and are not sensitive to temperature. Drawbacks consists on the lower cell voltage and poor voltage regulation.

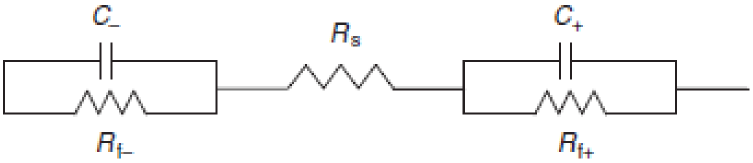

Figure 2.4: Lumped electrical model of a super-capacitor [11]

The one reported in figure 2.4 is the circuital model of a standard EDL capacitor: C_+ and C_- are the capacitances generated by each electrode, R_S is the equivalent series resistance of the cell and R_{f+} and R_{f-} are the Faradic resistance of electrodes, which are responsible for capacitor's discharge and are related to the electrode-electrolyte contact [11].

2.2 Electrolytes

Electrolytes are one of the main responsible for the good performances of a supercapacitor. The main challenges are to find a ”green” electrolyte able to guarantee the lower possible equivalent series resistance, an high capacitance and increase the specific energy density in order to make them comparable to batteries [14]. To increase this latter, we can act on C and V.

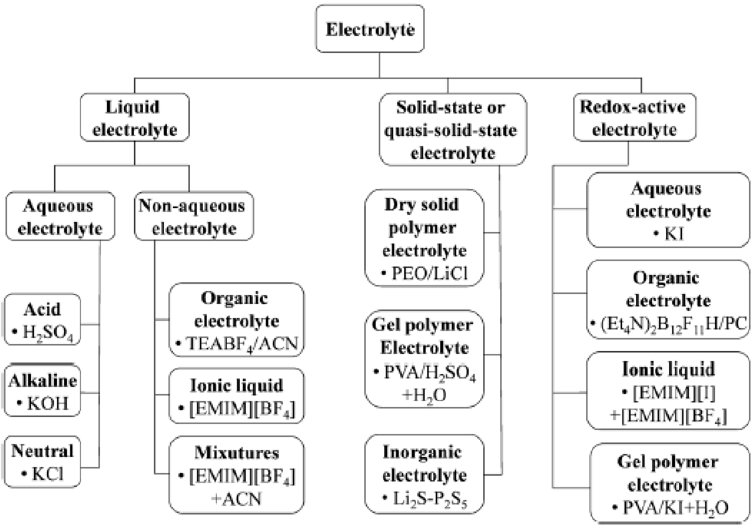

Figure 2.5: Scheme of all available type of electrolytes [14]

In specific, we have to guarantee the following properties:

- Wide potential window: from equation 2.3, we notice that increasing the voltage will cause a quadratic increase of the energy density. This will also increase the operating region of the device [11, 14].
- Guarantee the matching between pores dimensions (in case of EDLC) and the electrolyte dimensions: in this way we increase the capacitance of the entire device [11, 14].
- High ionic conductivity: this will reduce the ESR and so reduces losses and increases the maximum available power (from equation 2.4) [11, 14].
- High chemical and electrochemical stability: during the operation of the device we have to avoid degradation of the electrolyte due to reactions with electrodes or due to the voltage applied. If this is not guaranteed, we can observe malfunction of the device [11, 14].

- Wide operating temperature range: most potential application for super-capacitor is placed in the range -30°C and +70°C [11, 14]. Expanding the current working temperature range we can further widen the super-capacitor applications.
- Environmentally friendly and cheap [14]

We can have different types of electrolytes, depending on the type of super-capacitor we want and on the physical state of the electrolyte itself inside the device. In the following we will analyze them individually.

2.2.1 Liquid electrolytes

We can have a further division in this section, between water based electrolytes and non-aqueous electrolytes. The first category is characterized by a solution of a chemical composite dissolved in water. The solute can be an acid, an hydroxide or a salt. They can guarantee a good ionic conductivity reducing the equivalent series resistance, can be easily produced, safe to handle and are inexpensive. The specific capacitance that can be reached by the combination of different electrodes and electrolyte nature, depends also on the dimension of anions and cations inside the solvent. The most important drawback, is related to the low energy density a super-capacitor exploiting water based electrolyte can reach. This is caused by the narrow operating window of the device due to the water splitting phenomenon: over 1,2V water starts to split into hydrogen and oxygen, deteriorating the electrolyte which can cause corrosion of electrodes. Moreover, on the temperature side, the operation is limited by the freezing and boiling point of water [14].

On the other side, non aqueous electrolytes can be organic, ionic liquids or mixtures. All of these composites can reach higher operation windows, leading to an higher energy density and an higher power density compared to water based solutions, however we pay in terms of conductivity. Organic electrolytes are composed generally by conductive salt dissolved in acetonitrile or propylene carbonate solvent. They provide lower specific capacity, lower conductivity (higher ESR) compared to aqueous electrolytes. Moreover, they require specific purification and assembling processes in controlled environment [14].

Ionic liquids (IL) are salts composed only by ions, with a melting point below 100°C [14]. They are composed generally by an asymmetric organic cation and an inorganic or organic anion. They are characterized by high thermal stability, high tunability in terms of chemical and physical properties (thanks to their large variety), high electrochemical stability that makes them suitable for tolerate high voltages. Drawbacks are the high viscosity that reduces the conductivity, high costs of fabrication (they have to be manufactured in controlled environment with precise techniques) and lower specific capacitance with respect to aqueous and organic

electrolytes [14].
Finally mixtures are the latter category of liquid electrolytes: here we mix together ionic liquids and organic electrolytes, in order to reduce the viscosity and the equivalent series resistance. In this context, the ionic liquid is dissolved in the solvent of the organic compound, which provides to reduce the high viscosity typical of ionic liquids [14].

2.2.2 Solid or quasi-solid electrolytes

Due to the great demand of wearable devices, we require safe, strong and easy to manufacture devices. A solid electrolyte allows to avoid the use of a separator, since the electrolyte itself acts as a separator, reducing the complexity of fabrication, and provides a liquid-leakage free device.
Principal features a solid electrolyte has to guarantee are: high ionic conductivity, high stability (chemical, electrochemical and thermal) and high mechanical strength. It is possible to apply some further distinctions among this type of electrolytes:

- Solid polymer electrolyte: they are composed by a polymer and a salt without any kind of solvent, providing high mechanical strength. The ionic conductivity is given by the transportation of salt ions through the polymer. Disadvantages are low ionic conductivity and poor contact area between electrodes and electrolyte, leading to an high value of equivalent series resistance [14].

- Gel polymer electrolyte: they are composed by a polymeric matrix which acts as a host polymer, inside of which is dispersed a liquid electrolyte. In this way the transport happens through the solvent and not directly through the dry polymer. Because of the presence of a liquid solution inside this kind of polymers, they are also named quasi-solid electrolytes. Mechanically, we have poorer performances with respect to the SPE, but we gain in ionic conductivity, significantly higher with respect to the previous case. Of course, since the effective electrolyte is liquid, we have all advantages and drawbacks typically of liquid electrolytes, already mentioned in section 2.2.1. They can be used in flexible and wearable applications [14].

- Polyelectrolyte: are inorganic based composites, such as ceramics. These electrolytes are no bendable and characterized by no flexibility, but are thermally stable and mechanically strong. Some ceramics can provide high conductivity. Electrolyte-electrode contact can be improved exploiting carbon nanotubes [14].

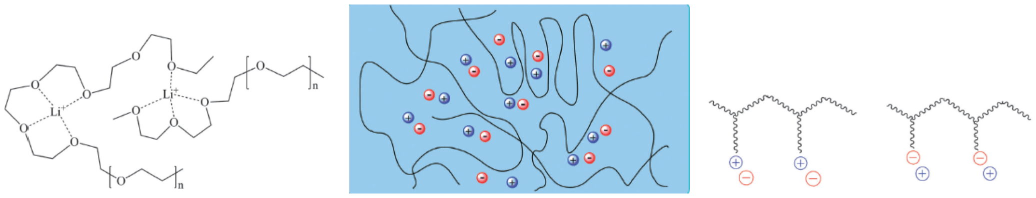

Figure 2.6: From left to right: the scheme of a solid polymer electrolyte, gel polymer electrolyte, polyelectrolyte [14]

2.2.3 Redox-active electrolytes

In order to increase as much as possible the capacitance of the device, we can exploit not only Faradic and non-Faradic phenomena happening at the electrode-electrolyte interface, but we can also profit from redox reactions occurring inside the electrolyte, providing in this way to an extra contribution to the overall capacitance.
Redox active aqueous electrolytes can be distinguished in 2 types, depending on the type of capacitance generated at the electrode: either it is an EDLC capacitor either it is a pseudo-capacitor. In general, all of them are based on iodides as redox mediators. However in both case we are able to increase in a significant way the capacitance of the device. Moreover in case of pseudo-capacitors we observe that the use of a redox-active electrolyte can lead to a speed up also to Faradic reactions at electrodes [14]. Cell voltage is subjected to all limitations typical of water.
In order to increase the power density and achieve an higher cell voltages, several organic and ionic liquid based redox-active electrolytes have been studied, leading to a significant contribution to the extra specific capacitance.
Also solid state redox active materials have been studied based on same redox mediators used in aqueous redox-active electrolytes which are dispersed as in GPE in a polymeric gel. Some enhanced performances have been observed: we have a much higher specific capacitance compared to standard GPE electrolytes.
All the solutions presented in this subsection can reach capacitances equals to thousands F/g, but it should be noticed that the overall capacitance is dominated by the electrode with lower capacitance, reaching anyway hundreds of F/g per device [14].

2.3 Binders and separators

Last elements to consider in a standard super-capacitors, are binders and separators. Those have structural employment, but can affect performances of the device if not properly selected. Binders are used in the creation of electrode layers, which in general are composed by powders or nano-particles. Binder must guarantee a good wettability of the electrode and good adhesion of it to current collectors. Most adopted binders nowadays are polyvinylidenefluoride, polytetrafluoroethylene and carboxymethylcellulose [14, 11]. Recent researches are directed to the selection of new environmentally-friendly binders, for example avoiding the use of fluorine.

Separators are used in order to prevent short circuits caused by contact between electrodes. They must have a low resistance for ionic conduction, have chemical and electrochemical stability inside the electrolyte and have a good mechanical strength to avoid mechanical issues. Most used materials are polymers, cellulose and glass fibres [14, 11]. The choice of a separator can also affect the range of the potential window of the device.

2.4 Membranes

Working principle of membranes is the same for both anionic and cationic selection: we couple a transport of electrical charges to a transport of mass exploiting a potential gradient applied from outside or internally generated [15].

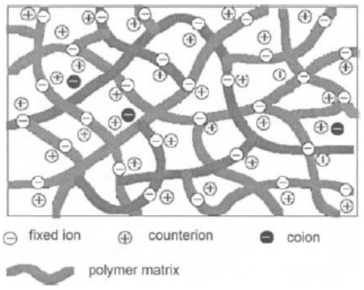

Figure 2.7: Scheme of a cation exchange membrane [15]

We can have 2 types of membranes, depending on the kind of ion we want to select. In particular in figure 2.7 is depicted a cation exchange membrane. Considering this case, we have a polymeric matrix over which are fixed negative charges which are in electrical equilibrium with external mobile ions. Since fixed ions are negative, they will attract positive external ions (called counter-ions), repelling all negative charges (called co-ions) because of Donnan exclusion. This kind of exclusion allows to propagate only positive ions. The same mechanism is adopted by AEM with inverted charges [15].

A good exchange membrane must be characterized by an high permselectivity (the ability to separate different components from each other), low electrical resistance and good mechanical, chemical and thermic stability. These features are nowadays satisfied by all commercial membranes, especially for what concerns the Nafion-based ones [15].

More in general, we can have 3 types of ion exchange process:

- Separation of components: here we separate acids, bases or salts from electrolyte solution. In this situation the driving force is an electrical potential, such as happens in electro-dialysis processes [15].
- Electrochemical reaction: at membrane surface we verify a chemical reaction which can generate chlorine, acids, bases, or organic/inorganic compounds that allow the passage of ions from one side to the other of the membrane [15].
- Conversion of chemical energy into electrical energy and vice-versa [15].

Most common applications of membranes are in electro-dialysis, desalination of water and membrane assisted capacitive mixing. All these techniques can be applied in many application's fields from biotechnology to energy production.

Chapter 3

Performances evaluation techniques

In order to evaluate the performances of a super-capacitor, we have to consider several parameters specific of a capacitive element. In particular, we have to evaluate cell capacitance, operating voltage and equivalent series resistance (ESR) [16]. From those parameters, it is possible to calculate time constant, power density and energy density through which we are able to place the device into a Ragone plot.

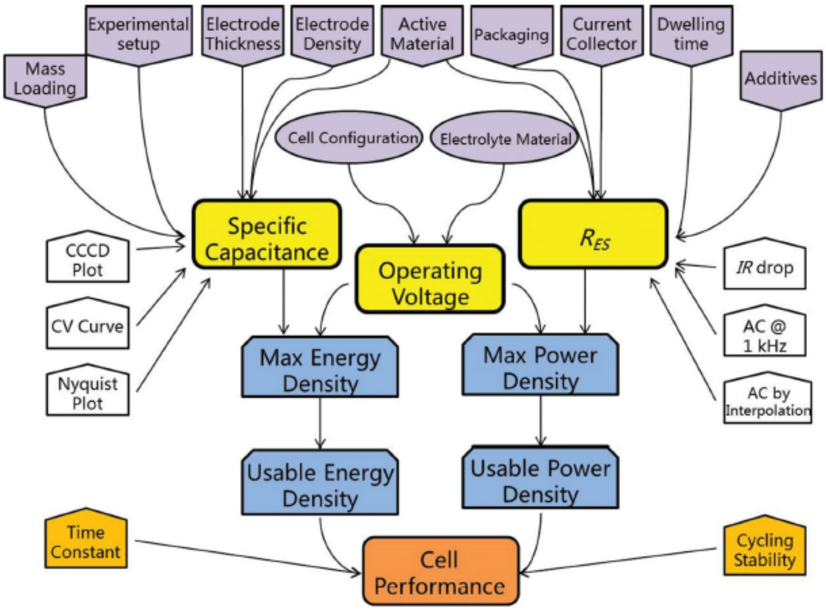

Figure 3.1: Schematic of parameters and techniques to evaluate them [16]

In figure 3.1, core parameters are underlined in yellow, in grey cell elements that can affect one (or more) of core parameters, in white technique we can exploit to analyze the device. Because of the many cross-relations between all the factors, the measure could be highly affected by the measurement setup adopted by the user. In first section are explained working principles of analysis techniques, then are analyzed methods to compute figures of merit used to characterize the device.

3.1 Techniques

In this thesis, the adopted techniques to characterize a cell are Cyclic voltammetry to evaluate the operating window, impedance spectroscopy for the ESR and constant current charge discharge to evaluate the capacitance.

3.1.1 Cyclic voltammetry

We have 2 different approaches for cyclic voltammetry (CV): we can have a two-electrode or a three-electrode configuration, depending on the type of evaluation we are interested in. In both cases, linear voltage sweep is applied to the setup, with a fixed velocity (scan rate, measured in mV/s). The amplitude of linear voltage sweep is the so called operating window [16]. The instantaneous current is recorded: its shape gives informations about the chemical reactions involved in the cycle.

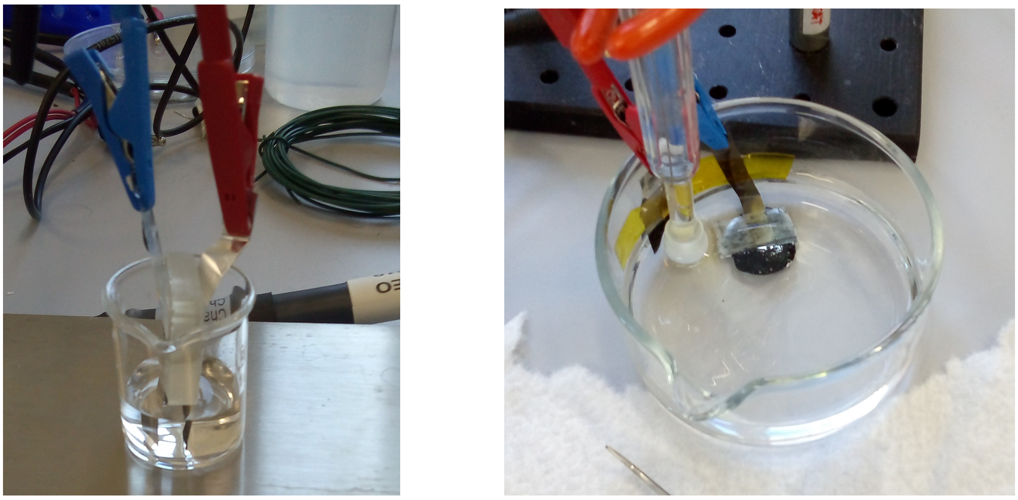

Figure 3.2: On the left two-electrode configuration, on the left three-electrode one

In figure 3.2 are depicted both the possible measurements setups. In the two-electrode configuration, we apply a voltage sweep between positive and negative electrode of the device with a fixed scan-rate. In this case we evaluate the characteristics of the whole cell. With the three-electrode configuration, the voltage is applied

between a working electrode (the one to be tested) and a reference electrode, which has an own stable potential. In this case we need a counter electrode, used in order to deliver the current requested by the working and closing in this way the circuit. In this configuration we evaluate the performances of a single electrode.
The obtained curve represents the current flow through the cell for a voltage swept over a certain voltage range [17]. Depending on the obtained shape of CV curve, we are able to understand if charge is stored through the creation of a double layer of charges, or it is due to chemical reactions. In EDL capacitors, we obtain a rectangular shape. When a reaction happens we observe a peak in the CV diagram. If the reaction is reversible, we can exploit that to increase the total capacitance, otherwise the performances of the device can be affected by this modification.
It is worth to notice that the instantaneous current due to EDL mechanism is proportional to the scan rate, while the one due to pseudo-capacitive mechanism is proportional to the square root of the scan rate [17]. Specific capacitance and energy performance can be computed by integrating the CV curves. In general the current follows equation 3.1.

$$I = \frac{dQ}{dt} = C\frac{dV}{dt} \tag{3.1}$$

As shown by equation 3.1, current is strongly dependent from the scan rate (dV/dt). A low scan rate allows slow processes to happen, but takes more time. An high scan rate provides faster analysis, but can affect the quality of measurements: high scan rate tests require more current and provide a capacitance lower than the capacitance obtained through low scan rate [17].
Theoretically for an EDLC, what we expect to obtain is an almost squared plot, as the one depicted below (3.3).

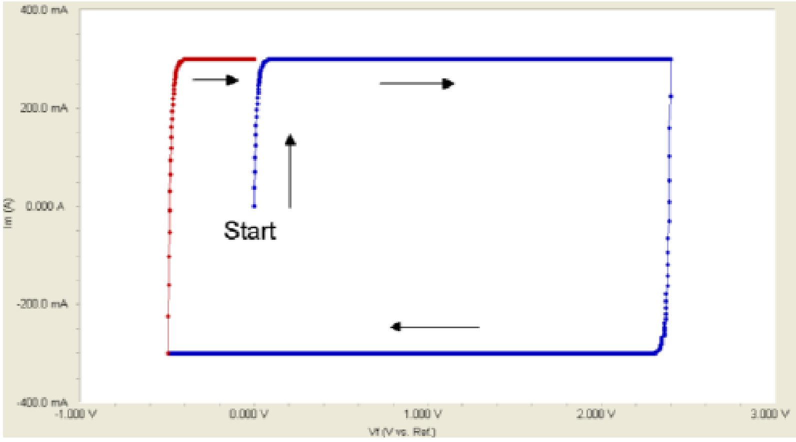

Figure 3.3: Theoretical shape of a CV curve [17]

Actually, since we deal with real and not ideal devices, we can encounter effect of ESR and the happening of redox (unwanted in EDLC) that can modify this ideal plot. In particular ESR makes the curve more slanting, whereas redox reactions produces rise of peaks.

3.1.2 Impedance spectroscopy

This measurement consists in the analysis of impedance spectrum. In general, a sinusoidal signal with 5 mV of peak amplitude is applied to the device with a frequency ranging from 1 MHz to 10 mHz [16]. Results can be then represented in a Bode diagram in order to show the frequency response of impedance, or in a Nyquist plot, where are reported real and imaginary part of the impedance in a complex plane.

This technique is particularly useful in the evaluation of equivalent series resistance (ESR): by convention, to compare the ESR between 2 devices, their impedance is evaluated at 1 KHz [16]. It must be reminded that this value is only a figure of merit to make a comparison and does not represent the effective value of ESR. ESR is defined as the value we obtain at the frequency that nullifies the imaginary part of the impedance. In this point the capacitive contribution is cancelled and we have only the resistive contribution. Real part of the impedance tells the amount of dissipation.

For an electrochemical cell, the adopted model is the Randles equivalent circuit in figure 3.4.

In this picture, real and imaginary part follow the relations:

$$Z' = R_S + \frac{R_{ct}}{1 + \omega^2 R_{ct}^2 C_{dl}^2} \qquad Z'' = \frac{R_{ct}^2 C_{dl} \omega}{1 + \omega^2 R_{ct}^2 C_{dl}^2} \tag{3.2}$$

R_S is the resistance due to the electrolyte, R_{ct} represents the charge transfer resistance (meaning the resistance experienced by electrons during motion), C_{dl} is the capacitance due to the double layer and X_W is the so called Warburg Element [18]. This last term takes into account the diffusion of ions inside the electrolyte during an electrochemical reaction: this is negligible for high frequencies, since ion migration takes much more time than the period of probe signal. Warburg element contribution is visible at low frequencies and is responsible for the behaviour of the right side of the Nyquist plot. At mid-high frequencies, we can observe the contribution of charge transfer resistance, while at high frequencies the last remaining term is R_S. Semi-circle portion of the Nyquist plot is due to the combined contribution of R_{ct} and C_{dl} [18].

We are mainly interested in behaviour of the device at low frequencies, so the right part of Nyquist. After the diffusion section, an ideal device Nyquist plot should

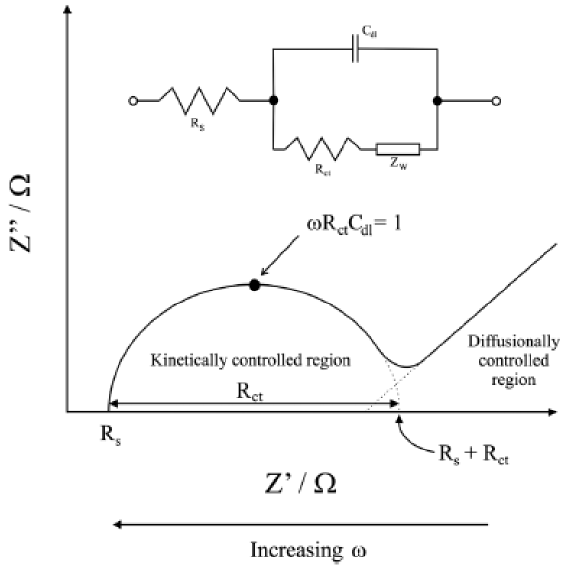

Figure 3.4: Nyquist plot and equivalent circuit of electrochemical cell [18]

become vertical. This would mean decoupling of resistance value from frequency (changing ω, Re[Z] remains constant).

3.1.3 Constant current charge/discharge

The CCCD is a direct current test, in which we apply a constant current to the device, which is maintained until reaching the total charge (discharge) of super-capacitor (or the working electrode): this threshold is setted by imposing a potential V_0 at which invert the current. Output is a plot of the potential versus time [16].
All core parameters of super-cap can be evaluated through this technique (capacitance, equivalent series resistance and operating voltage): exploiting them is possible to compute also other properties such as power density, time constant and energy density [19]. One of the advantages of CCCD technique is the possibility to evaluate directly capacitance and ESR of a super-cap without recurring to integrals, but only exploiting multiplication and divisions between known quantities.
In this type of characterization, the choice of current is crucial: a proper level of current must be adopted in order to produce consistent and comparable data from a CCCD test.
This technique can be adopted in order to obtain several other analysis, in particular:

- Cyclic stability: in this case, we pilot the super-capacitor with the maximum current the device admits and cycle for long time. In this way it is possible to evaluate how the characteristics of the super-capacitor changes after many working cycles and define its lifetime. In this case the general rule adopted to choose the current is to apply 1 A for each gram of active material.

- Float test: this test evaluates the ability of the device to maintain the charge. The principle is the same of the cyclic stability with a rest time after n charges/discharges. The rest time is greater than 10 hours and in this period is evaluated the change of the capacitance versus time.

3.2 Figures of merit

The direct output of previously described techniques is generally a plot of current versus voltage, or voltage versus time. Now the goal is to extrapolate from these results, the other characteristics.

3.2.1 Capacitance

By definition the capacitance is defined as the ratio between charge stored and the voltage at which the storage happened. In this way it is possible to evaluate the absolute total capacitance C_T. However as done with energy and power density in section 2.1, it is convenient to normalize also the capacitance to a particular feature of the electrode, named gravimetric capacitance C_S [11].

$$C_T = \frac{\mathit{\Delta} Q}{\mathit{\Delta} V} \qquad\qquad C_S = \frac{C_T}{\mathit{\Pi}} \tag{3.3}$$

In which $\mathit{\Pi}$ is a generic normalization factor (in particular can be the weight, volume, area or size of the electrode). For super-capacitors (in particular EDLC carbon based) the normalization factor is the weight of the active material. Otherwise the most common normalization factor is the area, however for carbon electrodes, but it is hard to compute the active area of active carbons because of their high porosity. Depending on the technique adopted, we have different ways to evaluate capacitance. In CV technique we need to solve the integral of current in time, in order to obtain the correct value of charge stored (released). Using CCCD, this is not requested, since the current is constant, so the amount of charge is computed as the product between current and time for which this is hold.

$$C_T = \frac{\int_{t(V_{min})}^{t(V_{MAX})} |I| dt}{2\mathit{\Delta} V} \tag{3.4}$$

$$C_T = \frac{I \times t}{\mathit{\Delta} V} \tag{3.5}$$

In equation 3.4, we have the integrand extremes represent the time at which we have the minimum voltage and the time at which we have the maximum voltage. In both equations (eq. 3.4 and 3.5), ΔV is the difference between maximum and minimum voltage, I is the instantaneous current.
Obviously, once obtained C_T, the evaluation of C_S is straight forward.

3.2.2 Equivalent series resistance

Exploiting a simpler model than the Randles one, we can say that a cell can be represented by series of a capacitance and a resistance (the ESR). This resistance is crucial in the definition of super-capacitor performance evaluation. Generally this is preferred to be the smallest possible [16]. Typical effect of an high ESR is the narrowing and slanting of CV curve, which becomes rhomboidal instead of rectangular.
The most widely accepted method to evaluate ESR is to exploit CCCD and analyze it in terms of IR drop:

$$ESR = \frac{V_{loss}}{I} \tag{3.6}$$

In which V_{loss} is voltage drop between charge and discharge section of the cycle [19]. This method however is not the most precise, and in general is avoided. IR drop is very affected by too many factors that makes measurement not reliable. For example one of these affecting factors is sample time: if not properly selected, sampling can strongly change the entity of the drop and so the evaluation of the ESR.
ESR can be also evaluated from EIS test as the real part of the complex impedance we have at 1 KHz (frequency which actually has been chosen for convention). Generally value from EIS is smaller than the value computed from CCCD [16, 19, 18]. Another way to evaluate ESR from EIS is to find the frequency at which the imaginary part of the impedance is null. At that point we have only the real part, which is effective ESR.

3.2.3 Operating voltage and Time constant

The operating voltage is the potential range within which a cell normally operates. It can be evaluated both with CV and CCCD, cycling with ΔV progressively higher. The maximum operating voltage is the last at which we have a regular shape of the cycle without any distortions. Those distortions can be spikes in CV or not negligible IR drops for CCCD. Operating voltage is strictly related (and in some cases limited) to the nature of the electrolyte and to the cell configuration [16].
Another parameter we need to compute is the time constant of a cell, which can be easily evaluated once known the equivalent series resistance and the total capacitance.

$$\tau = ESR \times C_T \tag{3.7}$$

A device characterized by a smaller τ provides a faster responsivity, that in some applications can be useful. For standard commercial Super-capacitors, time constant is comprised between 0,5 s and 3.6 s [16]. By definition, this is the time at which, considering the RC model, the device is 36% charged (discharged). After 4τ, we can consider the device fully charged (discharged).

3.2.4 Power and energy density

As underlined by Ragone plot, energy and power density are the fundamental 2 key parameters to define the operating region and the applications in which the device can be applied. These are the main parameters used for performance evaluation. Generally they are gravimetric definitions.

- Power density: maximum power delivered can be reached only with $R_{load} = ESR$ (matched load conditions) [16]. These conditions generally are not reached in working applications of the super-cap, but this convention has been taken as figure of merit.

  $$P_D = \frac{V_o^2}{4\Pi \times ESR} \tag{3.8}$$

  Above, V_o is the maximum operating window of the device and Π is the normalization factor (which can be both a weight or a volume).

- Energy density: this factor is related to the amount of energy a cell is able to store in a charging semi-cycle from $0V$ to V_o. It can be evaluated as

  $$E_D = \frac{1}{2\Pi} C_T V_o^2 \tag{3.9}$$

  Combining equations 3.6, 3.8 and 3.9 is possible to notice a strong coupling of energy and power density through time constant τ [16].

  $$\frac{E_D}{P_D} = 2C_T \times ESR = 2\tau \tag{3.10}$$

  This point is crucial, since the main issue is the lower energy density of super-capacitor, compared to batteries. If we want to increase E_D, we can act both on capacitance or operating voltage. Raising only capacitance, will also increase time constant, making the cell slower. The solution could be enlarge operating voltage, which increases both E_D and P_D, not affecting τ [16].

3.2.5 Coulombic efficiency

Last key parameter used to evaluate a cell performances is the coulombic efficiency, meaning the ability of a device to deliver almost all charge stored.

$$\eta = \frac{Q_{discharge}}{Q_{charge}} \tag{3.11}$$

This parameter can be computed exploiting both CV and CCCD techniques, by integrating in time charging and discharging current, so to obtain the amount of charges in both semi-cycles. This factor must always be the closest possible to 1, but it cannot be greater than 1.

Chapter 4

Membrane modified electrodes

The main idea is to reproduce the behaviour of device presented in section 1.4. The goal is to properly choose membranes characterized by good performances and possibly fluorine free. First analysis taken on is the evaluation of performances of an electrode over which we infiltrate a membrane. CV and EIS characterization are taken on exploiting a three electrodes configuration in a 1M KCl water solution. We exploit carbon electrodes over Ti current collectors. Reference is an Ag/AgCl electrode, finally the counter is a carbon pad. For preparations, see appendix A. Before all characterizations, membranes needed to be activated for a couple of hours in the used electrolyte.
All plots are normalized with respect to the mass of the active material (meaning activated carbons, neglecting membrane's mass).

4.1 Activated carbons

First thing to do, we have to characterize the behaviour of a carbon electrode, in order to obtain a figure of merit to refer to for comparisons. As we can notice from the FESEM acquisitions, we can clearly see the grainy nature of activated carbons (AC) and observe porosity on the surface of the electrode.

As we know, we should consider also the capacitance of Ti in parallel to the capacitance of activated carbons, so we perform a CV also for a current collector without any covering and normalizing to the surface.

If we compare the obtained capacitance (in figure 4.2) to the one of AC (in this particular case normalized to surface, in figure 4.3), we find the contribution due to titanium is absolutely negligible.

Once we become aware of this fact, we can evaluate the real figures of merit we have to compare with. These are: CV curves, EIS spectrography, Capacitance plot and Coulombic efficiency.

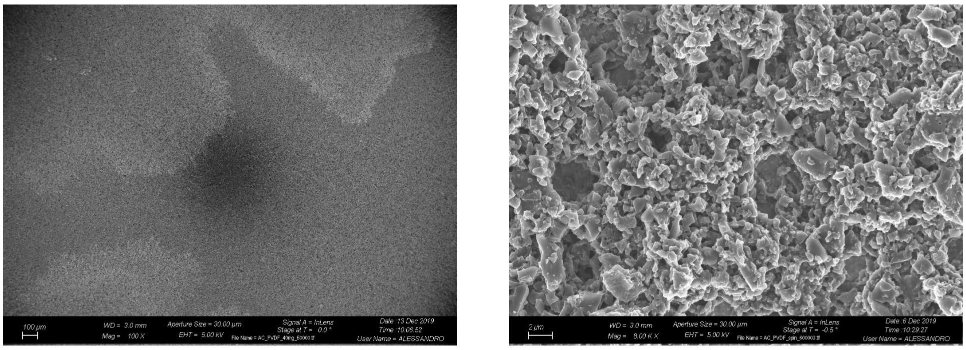

Figure 4.1: FESEM picture of activated carbons on Ti with PVDF binder

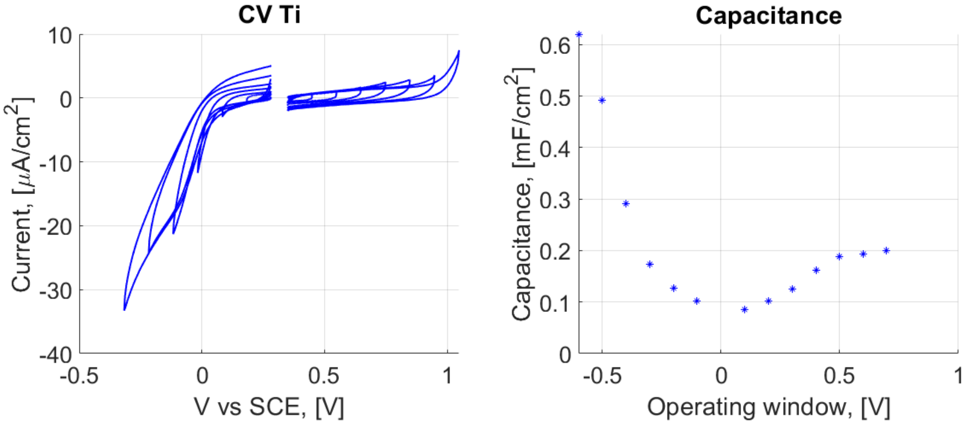

Figure 4.2: Titanium capacitance evaluation

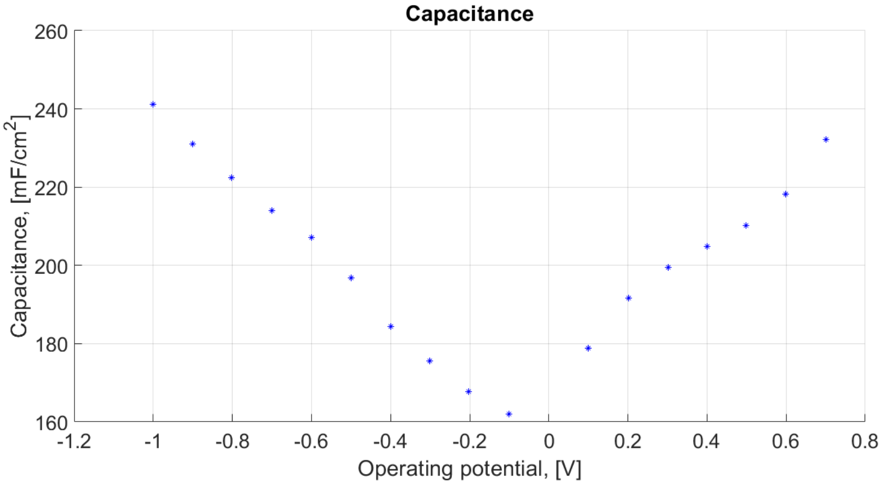

Figure 4.3: AC capacitance evaluation per surface

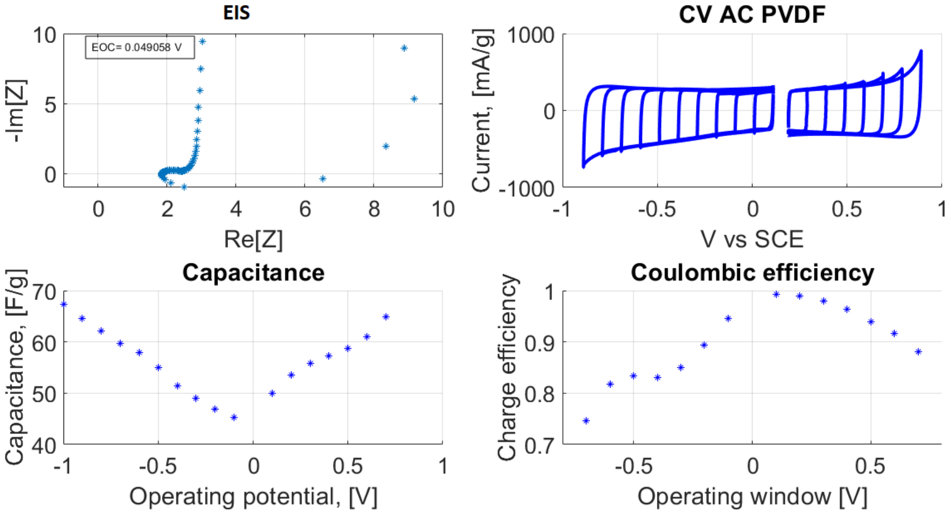

Figure 4.4: AC EIS and CV

From the obtained plots, we can say that operating window ranges for 0,4 V on the positive side, and for 0,7 V on the negative side, having a capacitance of 60 F/g and a series resistance equal to 1,8 *Ω*.

4.2 Infiltrated membrane

This characterization represents an innovation since in all previously analyzed membrane based processes, membranes are leaned on electrodes, contributing to the enhance of series resistance and contain the reduction of the capacitance. The infiltration process consists into melting the membrane, deposing it on the carbon based electrode and then dry the solution in order to have a uniform coating. For the first step, we exploit dimethyl-sulfoxide, which is the solvent able to melt membranes we want to depose (concentration of 40 mg/mL).
First approach adopted to infiltrate consisted into depose DMSO-membrane solution by means of a pipette while the electrode stands onto an hot plate heated at 60°C. In this way we have to perform several depositions (4/5) before reaching an acceptable covering of the substrate. The low temperature makes the process time consuming, since we cannot proceed to a new deposition while the previous one is not perfectly dried. However even if we have a sufficient coverage of the electrode, the result is poor in terms of uniformity: we have regions in which the membrane is too much concentrated and regions where activated carbons are not covered.
Second attempt to obtain a better coverage, was to exploit spin coating technique. In this configuration, however, we cannot obtain any covering since membranes are

not able to remain attached to the electrode. Have been attempts at low rpm, high rpm, with a pre-deposition before spin coating, but all of them gave the same negative result, so this technique is not effective in this case.
Third and finally adopted approach is similar to the first one, but requiring only 2 depositions. We exploit the 40 mg/mL solution of membrane in DMSO, deposing it on an electrode placed on an hot plate heated at 100°C for the first depositions, once DMSO is dried, we can proceed to second deposition, raising temperature at 130°C. If temperature is higher, this process could lead to small cracks in the activated carbons, but if properly controlled, we can achieve a good coverage.

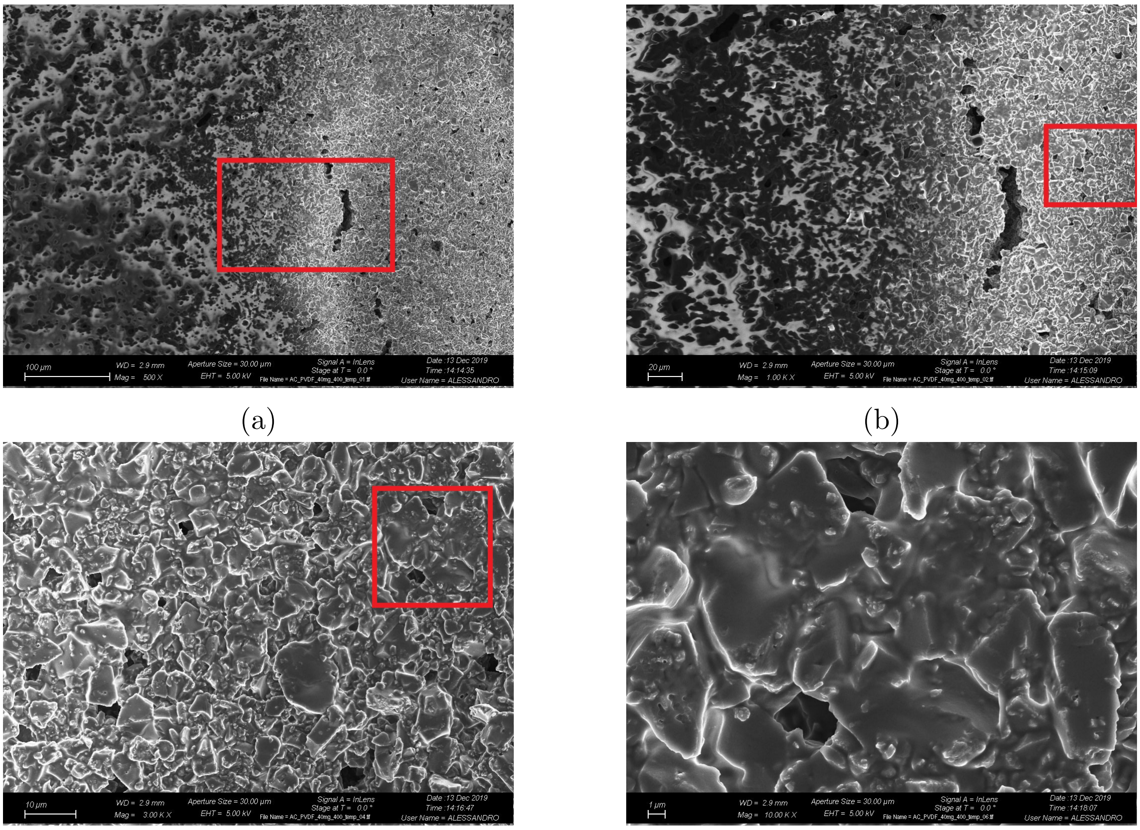

(a) (b) (c) (d)

Figure 4.5: Fesem images of infiltrated activated carbons

In figures 4.5, we can observe how the infiltration appears with different magnifications. In figure 4.5a, we can clearly identify 2 regions: the lighter region is the one where we have an optimal thin coverage, while in the darker region, polymer is thicker.
Even better results are achieved exploiting a Büchi glass oven system: with this setup we are able to heat the electrode at low pressure. In this way we are able to

avoid the trap of gas inside carbon pores, generating contemporarily a more uniform coverage of activated carbons. Images are presented in figure 4.6.

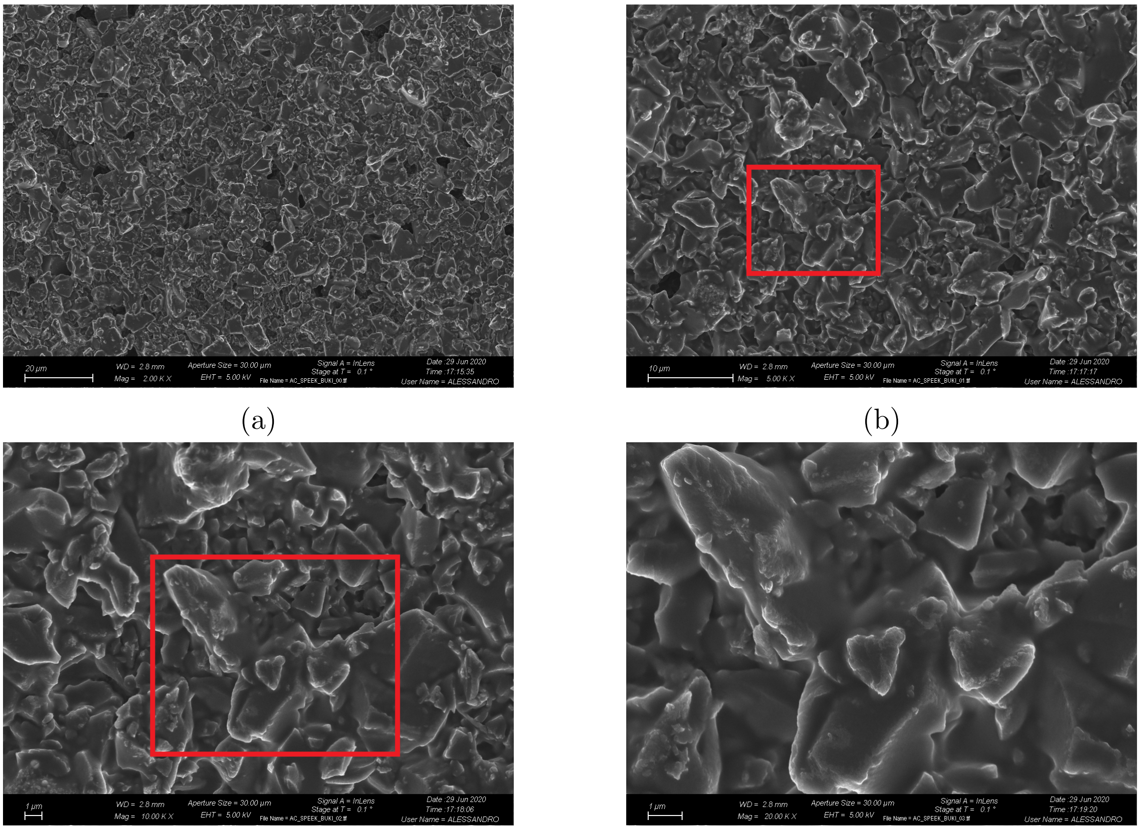

(a) (b) (c) (d)

Figure 4.6: Fesem images of infiltrated activated carbons through Büki

Studied membranes are both cationic and anionic:

- DABCO 1 (anionic)
- DABCO 2 (anionic)
- SPES (cationic)
- SPEEK (cationic)
- SPES-SPEEK (cationic)

4.2.1 Anionic exchange membranes

This kind of membrane allows the passage of anions (negative charges), so it has to be placed on the positive electrode of the device, so to allow an auto-generative charging.
Generally the main problem with anionic exchange membrane (AEM) is related to the low conductivity and low chemical stability to alkali and at high temperature [20]. In order to solve this issue, cross-linking processes are adopted. Cross-linking is a chemical process in which we exploit so called ”cross-linking reagents” [21], able to produce covalent bondings between membrane components. In this way we are able to increase the chemical stability of the whole membrane.
Backbone polymer adopted for anionic exchange membranes is PES (polyether sulfone).

DABCO 1

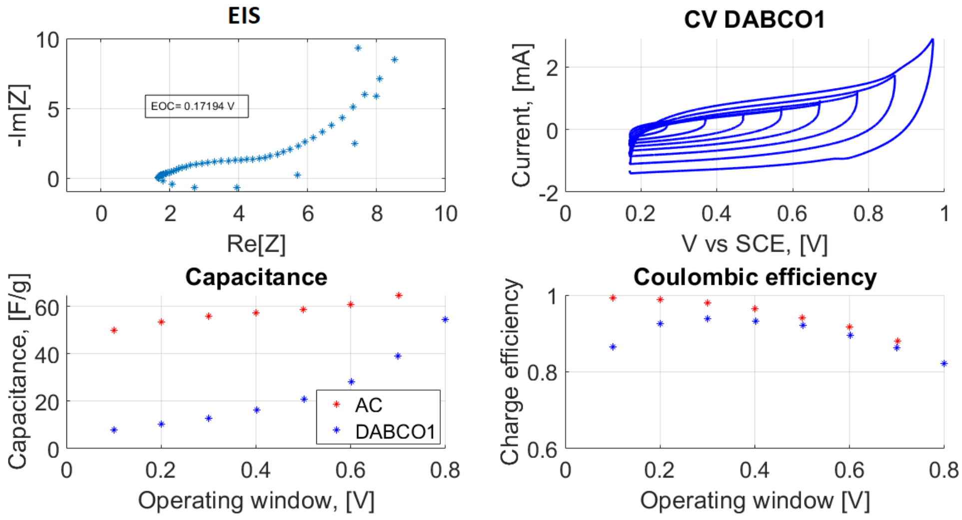

Figure 4.7: Characteristics of DABCO 1 membrane

In above figure, we can notice a good ESR, since it can be considered the same we obtained for uncoated activated carbons, but we notice a strong decreasing in capacitance (decrease from 20 to 40 F/g compared to uncoated carbons). Coulombic efficiency can be considered stable with respect to activated carbons.

DABCO 2

In figure 4.8, we can observe a modest increase in ESR (few tenths of Ω). Cyclic voltammetry, capacitance and charge efficiency does not change so much compared

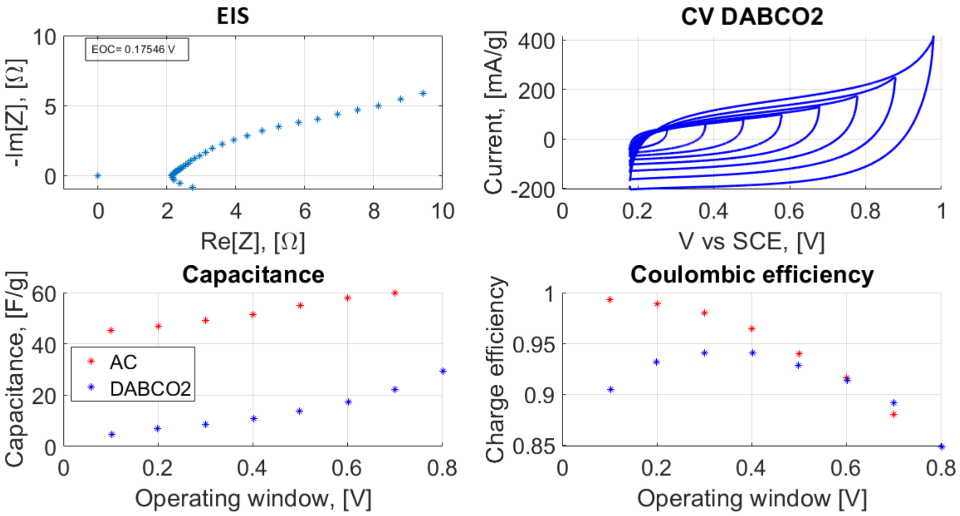

Figure 4.8: Characteristics of DABCO 2 membrane

to figure 4.7. Among these membranes it is hard to choose one, because there is no evidence of better performances of DABCO 1 rather than DABCO 2. Moreover, if we consider only PEIS of both membranes (figure 4.7, 4.8), we can notice haw at low frequencies we still have an high dependence of Re[Z] from frequency.
Difference between this membrane and the previous one is in chloromethylation process adopted. For anionic membranes it is easier to use a polysulfone backbone (PSU) respect to a PES one.

4.2.2 Cationic exchange membranes

Cationic exchange membranes (CEM) allows the passage of positive charges. This means that we have to place them on negative electrode (cathode). Most widely used and commercialized CEM are Nafion based ones, however it presents some drawbacks leading to the idea of finding something alternative [22]. In particular Nafion is obtained exploiting high cost reagents such as Platinum, it can release carbon monoxide during the operating, and most of all it is composed by a large amount of Fluorine, which is toxic and polluting for the environment.
Actually it is possible to synthesize new membranes able to reach a conductivity comparable to the one of Nafion. In particular, we can adopt SPEEK and SPES membranes which overall have no fluorine inside of them.
In this case, instead of a cross-link process, the needed process is called sulfonation which adds sulfunate groups to the chain. These groups will be then responsible for good cation transport and increase hydrophilicity of the membrane [23, 22].
In general a good membrane has to guarantee an high ionic conductivity, minimal

water/methanol transport, high mechanical strength, high resistance to oxidation, reduction and hydrolysis [22].

SPES

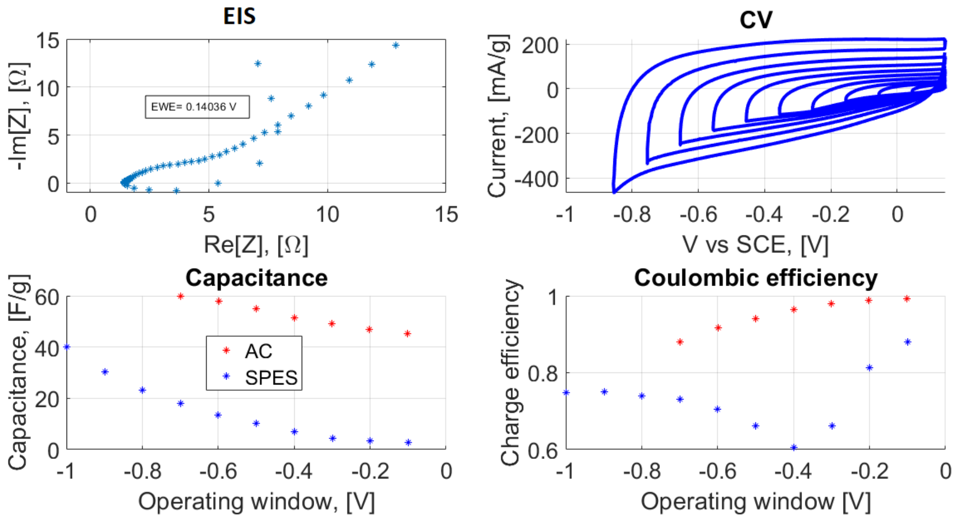

Figure 4.9: Characteristics of SPES membrane

As decided for anionic exchange membranes, also for CEM the first attempt was to exploit PES as backbone polymer for the entire membrane. Characteristics of SPES are high glass transition temperature, high chemical, thermal and mechanical resistance. However, the polyethersulfone is hydrophobic and sensitive to many organic solvents [24].
Also in this case (as happened for AEM), the choice of polyether sulfone is not the right one, since we have a low Coulombic efficiency and an high decrease of capacitance. Cyclic voltammetry curves shows an high deformation, if compared to CV of pure activated carbons and real part of impedance is strongly affected by the frequency. The only good result is the maintain of an ESR comparable to AC, at 1,5 Ω.

SPEEK

Polyether ether ketone is an high performances engineering thermoplastic with good solvent resistance and thermal and chemical stability, making it a good alternative to Nafion based membranes [23].
If we analyze figure 4.10, we can notice good results for CV curves, ESR and Coulombic efficiency. Resistance is not affected by the presence of the membrane and

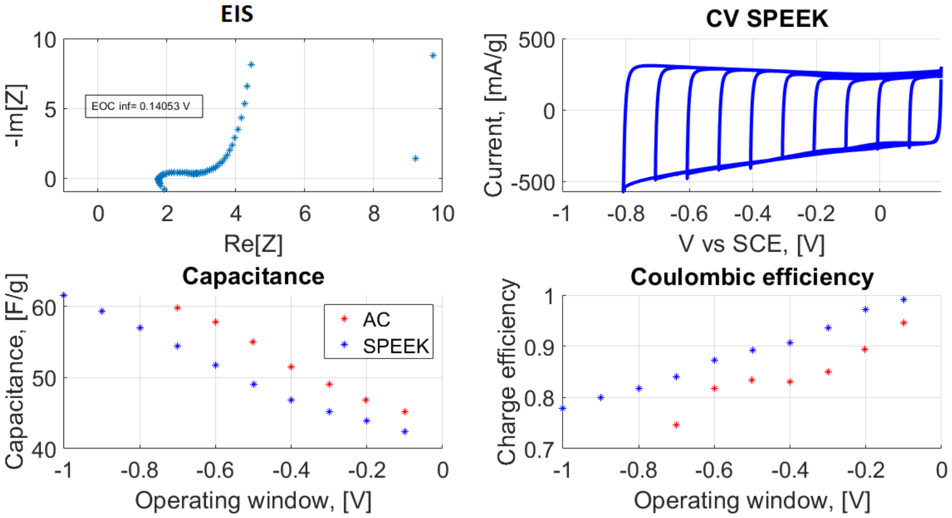

Figure 4.10: Characteristics of SPEEK membrane

remains constant for middle-low frequencies. Moreover, cyclic voltammetry curves have the same shape obtained with activated carbons and if we analyze coulombic efficiency, this is slightly increased by the presence of SPEEK.
The drawback is related to the reduction of the overall capacitance (average loss of 10 F/g), since the membrane infiltrated over the electrode closes pores, reducing the active area of the electrode. However until now, the values of capacitance reached are the higher obtained.

SPES-SPEEK

For this kind of membrane, the process consist in mixing together PES and PEEK polymers and then proceed to the sulfonation of both polymers together. Result is a trade off between 2 previous results. CV is a slightly less deformed and Coulombic efficiency is comparable to activated carbons. We do not have bad results, but they are worse than the ones reported in section 4.2.2.

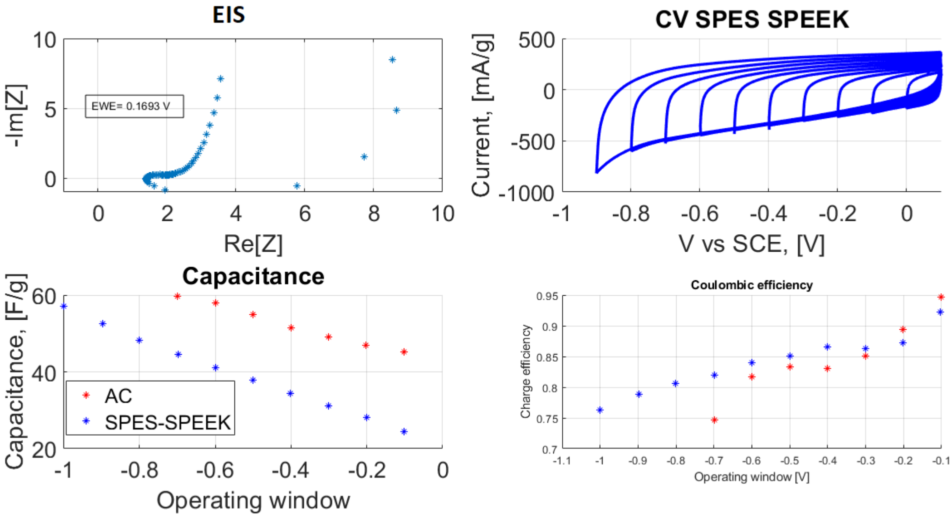

Figure 4.11: Characteristics of SPES-SPEEK membrane

4.3 Leaned membrane

Recalling lumped model of the super-capacitor, as depicted by [11] in figure 2.4, we can notice that resulting capacitance is the series of capacitances due to both electrodes. This value,is limited by the value of smaller capacitance electrode, since:

$$C_{tot} = \left(\frac{1}{C_+}\right)^{-1} + \left(\frac{1}{C_-}\right)^{-1} \tag{4.1}$$

Analyzing obtained results in previous section, we can say that the only good result has been achieved for SPEEK membrane. So, for the moment, the decision was to build a device characterized by a pure activated carbon anode and a SPEEK modified cathode. In this way we can ensure that working is not affected by the presence of a poor quality anion exchange membrane.
Before building a device so intended, it is useful to compare performances of an electrode modified through infiltration and leaning.
Leaning membrane on electrode, we have to pay attention there is present electrolyte between electrode and membrane, but there is no path through the electrolyte that connects directly working and counter electrode. This is done by placing a capton strip behind collector and on the other side place the membrane, so to cover and sealing all activated carbons (figure 4.12).

Then, using a pipe, we insert electrolyte in the so formed ”pocket”. We have to avoid the contact between electrolyte inside the ”pocket” an electrolyte outside.

In figure 4.13, are reported results of an electrode with leaned membrane (taken from the same sample used in section 4.2.2). Analyzing the obtained results, we

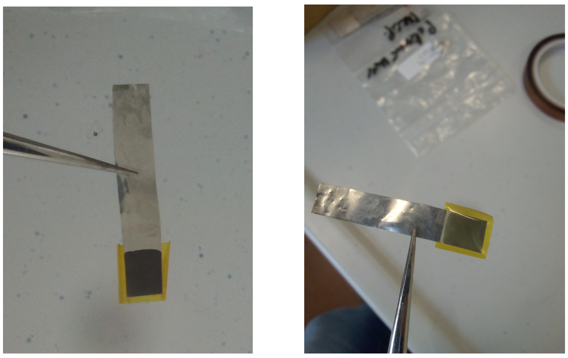

Figure 4.12: Leaning of a membrane over a carbon electrode.

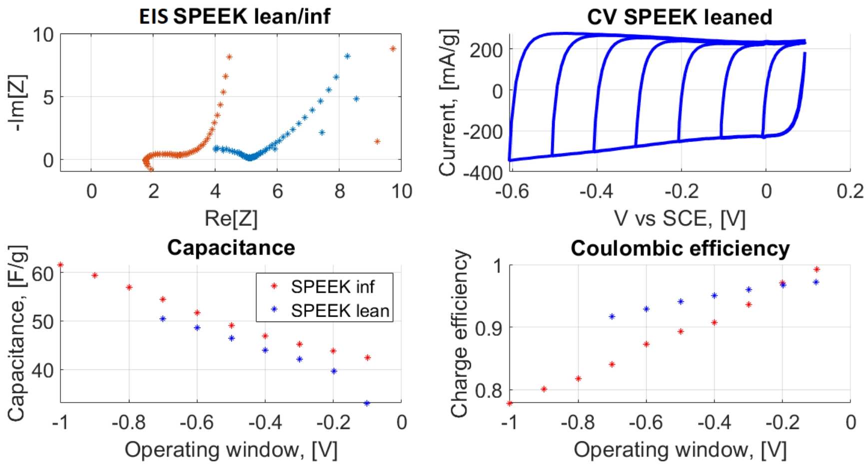

Figure 4.13: Comparison between infiltrated SPEEK and leaned one

can notice several improvements: first of all, observing the Nyquist plot, we can notice how the ESR of infiltrated membrane is half of the ESR of the leaned one (1,5 Ω versus 3 Ω, value obtained by interpolating electrochemical circle in order to find intersection with -Im(Z)=0) and at low frequencies, leaned membrane electrode shows a more dispersive behaviour. CV curve in 4.13 is not so sharp compared to figure 4.10, but most important result is that we were able to reproduce same capacitances obtained with leaning even with infiltration. Drawback is a slight loss in Coulombic efficiency: leaned membrane efficiency is higher than infiltrated membrane one (which however remains higher than uncoated activated carbons).
Finally we can conclude that infiltrating a membrane is a good idea since we can obtain the same capacitances of the same membrane leaned and reduce a lot the resistive contribution, paying only from efficiency point of view, which however is improved compared to uncoated carbons case.

Chapter 5

SPEEK as binder instead of PVDF

Since SPEEK is a polymer able to be melted and dried in order to form long chains, the idea was to substitute poly-vinylidene fluoride (PVDF) as the binder of cathode with SPEEK itself. In this way we can obtain a good attachment of activated carbons to the substrate and guarantee a first type of charge selection. Moreover in this way we are able to avoid the use of fluorine at least for one of the two electrodes, so reducing costs and environmental impact.
In order to find the best percentage of SPEEK and activated carbons, we studied some configurations: 90% AC - 10% SPEEK, 80% AC - 20% SPEEK, 70% AC - 30% SPEEK, 50% AC - 50% SPEEK. All of these attempts (but 80% 20% composition) where morphologically and electrochemically characterized.

5.1 90% AC - 10% SPEEK

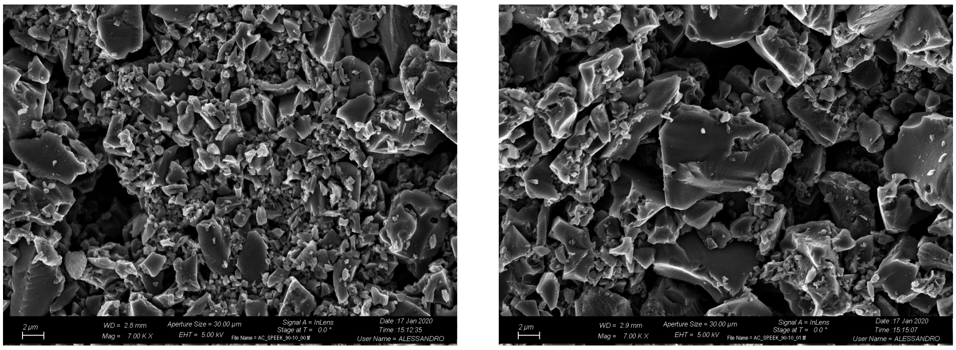

Figure 5.1: FESEM picture of 90% AC and 10% SPEEK

In figure 5.1, we can observe no SPEEK, and the acquisition is strictly similar to image 4.1: this probably means that binder will not affect total capacitance of the electrode, since all previous pores are maintained open also in this configuration. Considering electrochemical analysis, they are reported in figure 5.2. We find a resistance comparable to the resistance of activated carbons, but better results are achieved for what concerns capacitance and coulombic efficiency: in both cases we have higher values with respect to figure 4.4.This composition could represent a good alternative to PVDF electrodes, since with a light increase of ESR, we are able to improve both capacitance and efficiency.

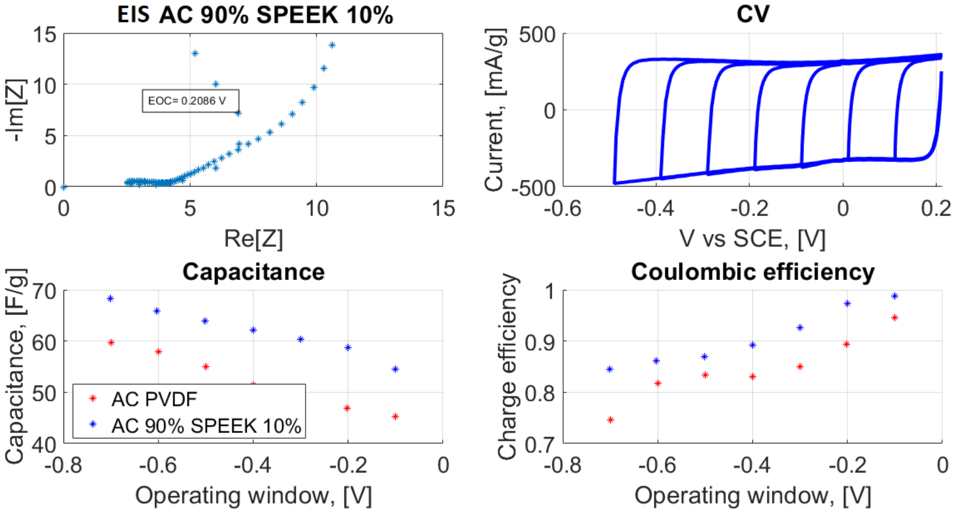

Figure 5.2: Characteristics of AC 90% SPEEK 10% electrode

5.2 80% AC - 20% SPEEK

In this case, we do not performed a morphological analysis since this step was added after characterization of all other compositions, in order to have a further confirmation of observed trend during property analysis vs percentage of binder. Here we present only electrochemical performances.

Here (figure 5.3) we can notice how resistance due to this electrode is very similar to the one depicted in figure 5.2. However one has to note also how the capacitance is reduced below pure activated carbons electrode and efficiency becomes comparable to the efficiency of AC.

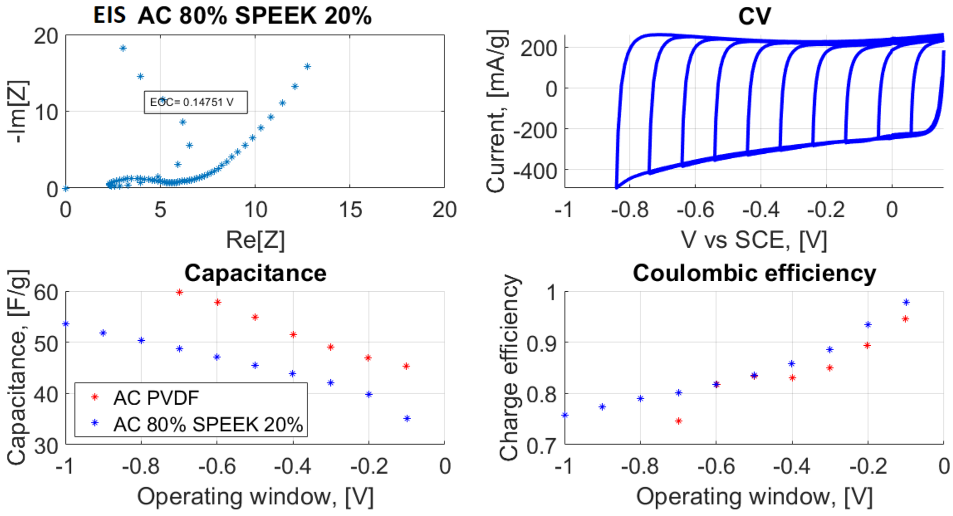

Figure 5.3: Characteristics of AC 80% SPEEK 20% electrode

5.3 70% AC - 30% SPEEK

In acquisition 5.4, we can clearly see activated carbons grains in foreground, where in background it is possible to find SPEEK structures.

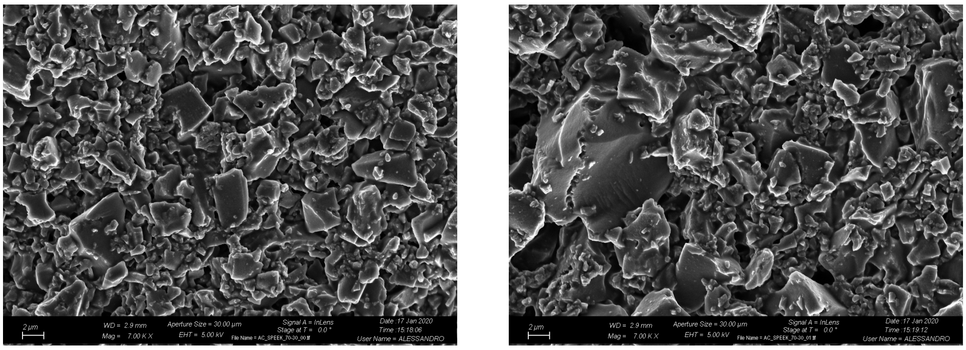

Figure 5.4: FESEM picture of 70% AC and 30% SPEEK

What we will expect is a more selective electrode, but with a further reduce of total capacitance.

Results depicted in figure 5.5, confirm previsions: electrode resistance is still ranging around 2 Ω, the higher drawback is the reduction of the total output current which is reduced with respect to both previous compositions. This affects total capacitance value of the entire electrode.

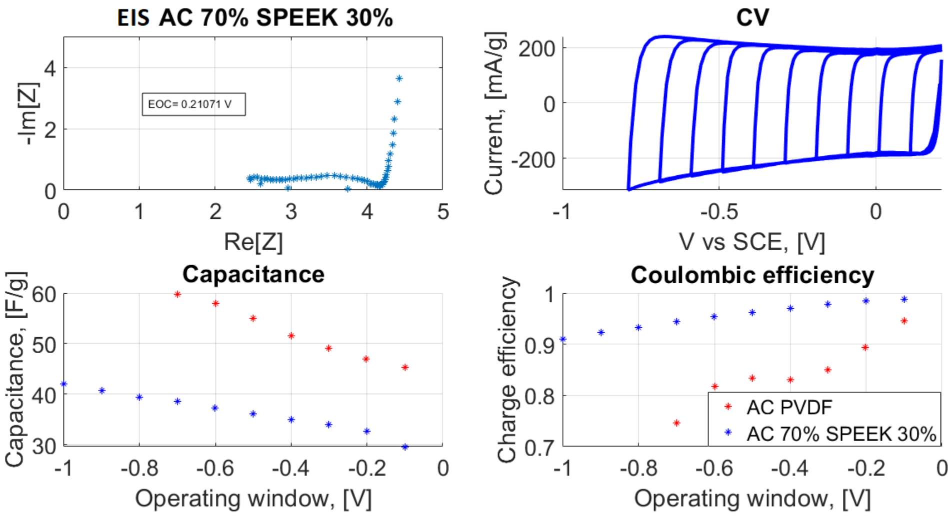

Figure 5.5: Characteristics of AC 70% SPEEK 30% electrode

Interesting results can be observed when we analyze Coulombic efficiency which is the higher we have reached until now, which is even higher than the efficiency reached with leaned membrane (figure 4.13). Below (figure 5.6) is depicted the direct comparison between Coulombic efficiency of the leaned membrane electrode and the 70%-30% composition.

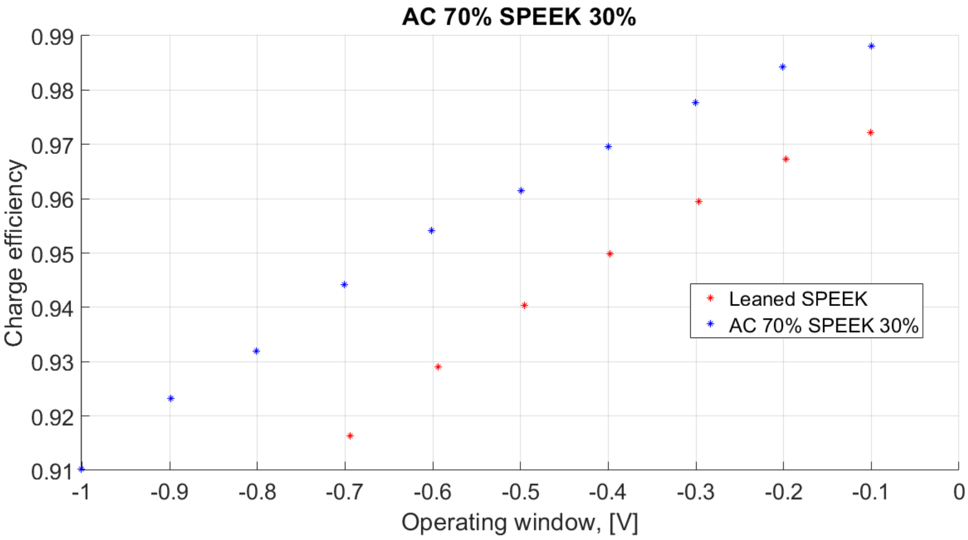

Figure 5.6: Comparison between leaned membrane electrode and 70%-30% composition

5.4 50% AC - 50% SPEEK

In this section, we have the same amount of polymer and activated carbons. In figure 5.7, we can clearly observe how polymer not only glues AC to the current collector, but also covers all surface of the electrode as already observed in figure 4.5.

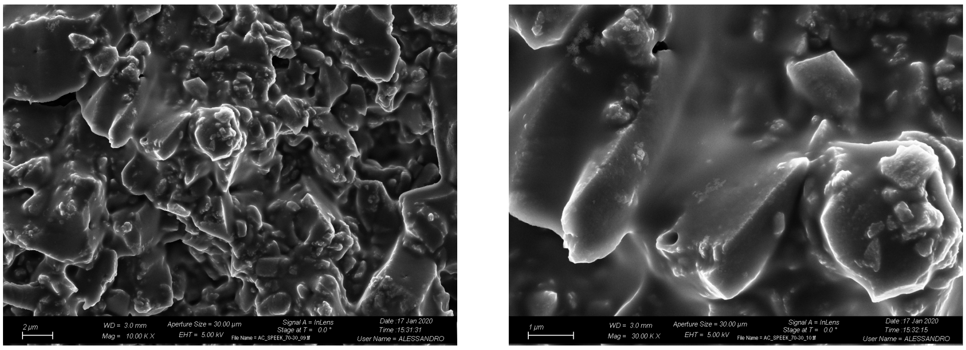

Figure 5.7: FESEM picture of 50% AC and 50% SPEEK

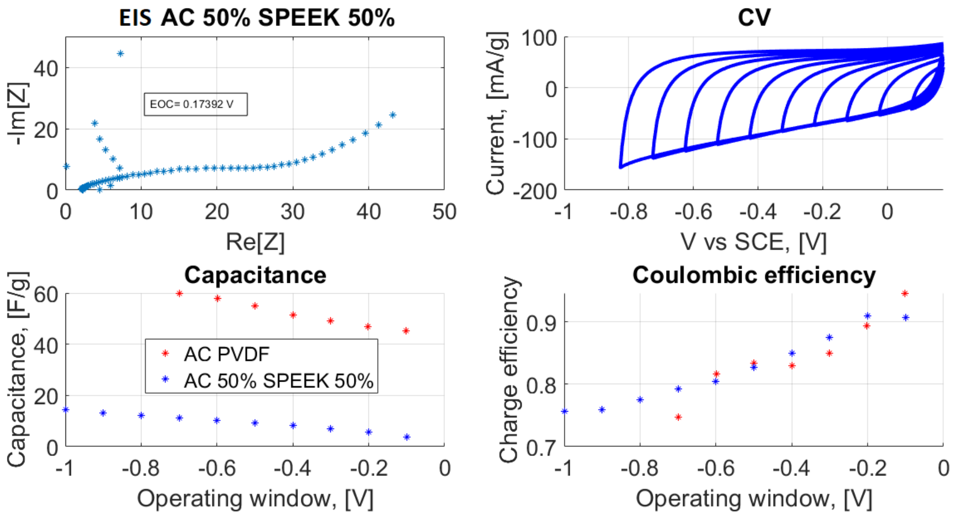

Figure 5.8: Characteristics of AC 50% SPEEK 50% electrode

In figure 5.8 we can notice how the resistance is not increased, but remains constant at 2 *Ω* whereas for total output current we have a drastic reduction, since we have now a maximum excursion of 150 mA/g at the applied voltage of -0,7 V, when for 90% AC 10% SPEEK composition, at the same voltage we had and excursion of 700 mA/g (figure 5.2). Moreover, CV curves are strongly distorted and capacitance is even lower than the SPEEK infiltrated electrode (reduction of about 10 F/g, figure 4.10).

5.5 Synoptic overview

In this last section of this chapter, we try to select the proper composition for our purposes. In order to do that, we exploit the following graph (5.9).

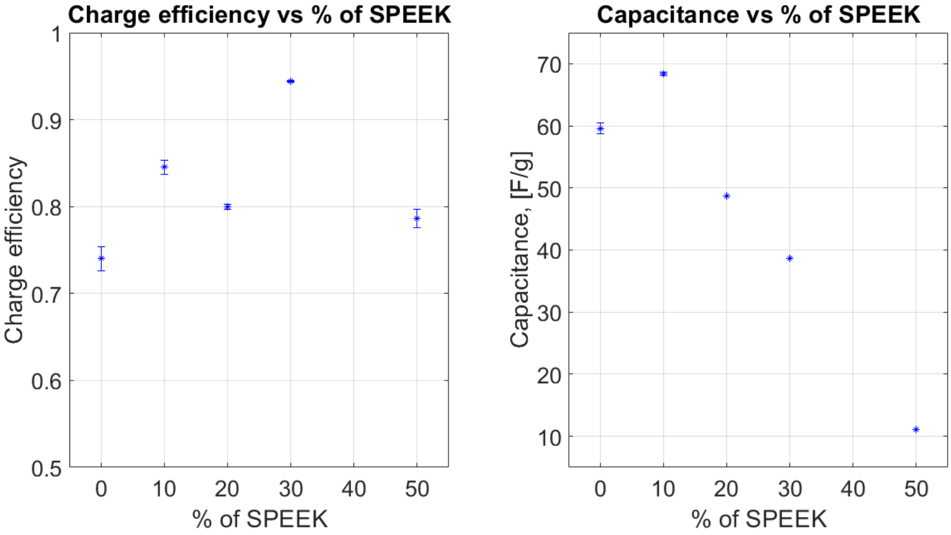

Figure 5.9: Comparison of Charge efficiency and capacitance VS percentage of SPEEK

Where is written percentage of SPEEK=0%, it is intended the performance obtained with activated carbons with PVDF binder. All data are collected for CV curve ranging from 0 V to -0,7 V.
As noticed also before, we have the best performances in terms of charge efficiency for 30% of SPEEK and best performances in terms of capacitance for 10% of SPEEK. This means that for our purposes, we can adopt 90% activated carbons 10% SPEEK composition, since we have no increase of resistance, but increase of charge efficiency and increase of capacitance compared to pure activated carbons. All these considerations are only valid in cathodic region.
The other noticeable composition (70% activated carbons 30% SPEEK) can be exploited in applications where are needed high efficiencies (near 95% at -0.7V) and are no required high capacitances.

Chapter 6

Cell configuration: 2 electrodes analysis

At this point, once selected SPEEK membrane for cathode and noticed the poor quality of anion exchange membrane for the anode, we are able to build a cell with 2 electrodes and evaluate its performances. We will analyze some different configurations. All CV measurements are carried on at different scan rates, in particular those are 1 mV/s, 5 mV/s, 10 mV/s, 20 mV/s, 50 mV/s. For what concerns CCCD, current selected is 0,5 A for each device.

6.1 AC PVDF - AC PVDF

This is the reference to which compare all results. This has to be considered the basis cell configuration to which apply our modifications.

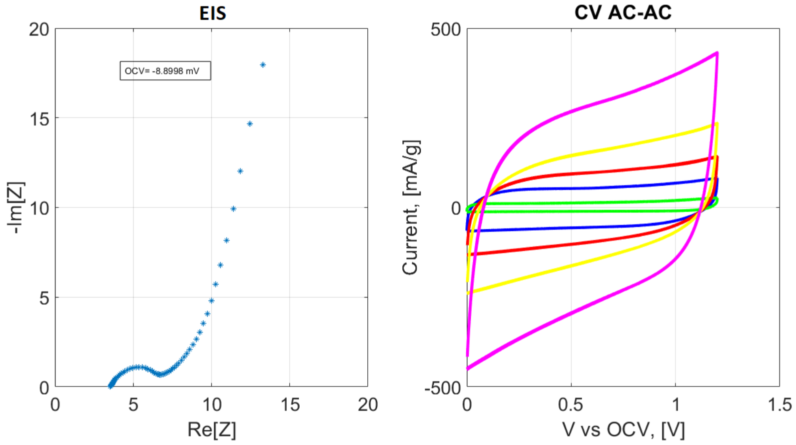

Figure 6.1: Characteristics of AC - AC device (PVDF as binder for both electrodes)

In particular, here we have to notice the ESR of the device which is equal to twice the resistance due to a single activated carbon electrode, around 4 Ω. Capacitance is equal to about 15 F/g with efficiency of 85%. Right side of Nyquist plot shows also a good shape.
In the following table are summarized all key parameters: C is capacitance from CCCD, ESR is obtained through EIS, τ is time constant, E_d is energy density, P_d is power density, η is the Coulombic efficiency.

C [F/g]	ESR [Ω]	τ [s]	E_d [Wh/kg]	P_d [kW/kg]	η [%]
11,9	3.45	0,6786	2,36	6,262	85,2

6.2 AC PVDF - AC PVDF with infiltrated SPEEK

In section 6.1, no matter choice we make in polarizing device, since both electrodes are the same. Now, we had modified one electrode, making the entire device asymmetric. So we have to pay attention where the place positive and negative contact. In particular we have to ensure AC PVDF electrode is the anode (positive electrode) and the SPEEK modified one is cathode (negative electrode).

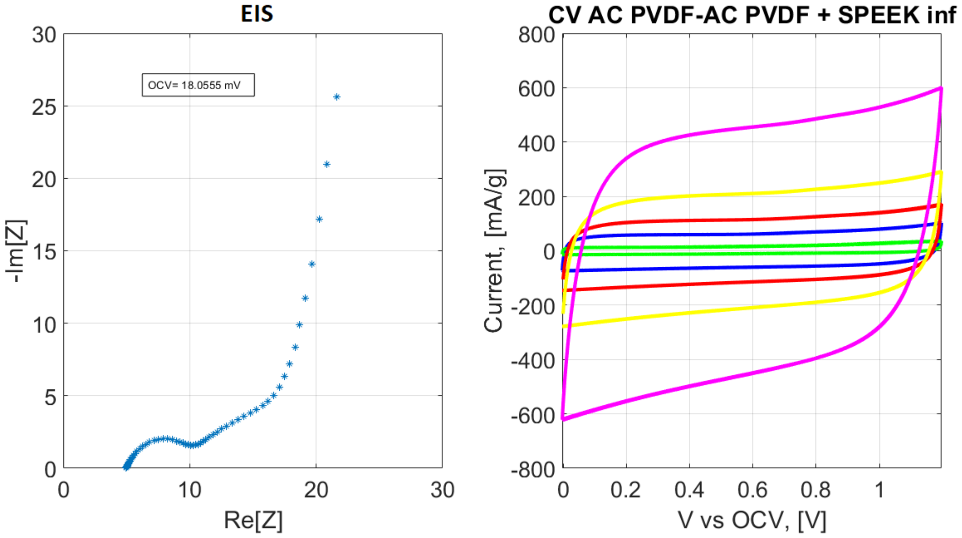

Figure 6.2: Characteristics of AC - AC+SPEEK device (PVDF as binder for both electrodes)

In this configuration we have an increase of ESR and a reduction of quality regarding low frequency performance. Considering CCCD analysis performed with a current of 40 mA/g between 0 V and 1,2 V, we obtain a capacitance equal to 12,4 F/g and a Coulombic efficiency equal to 90%. Capacitance is almost the same and

the efficiency is maintained pretty well.
Following we have the summarize of key parameters.

C [F/g]	ESR [Ω]	τ [s]	E_d [Wh/kg]	P_d [kW/kg]	η [%]
12,4	4,87	0,4473	2,45	9,864	89,8

6.3 AC PVDF - AC 90% SPEEK 10%

In this case we exploit SPEEK as binder for cathode electrode, so even there we have to pay attention to the polarization, since also binder introduces a first rough charge selectivity.

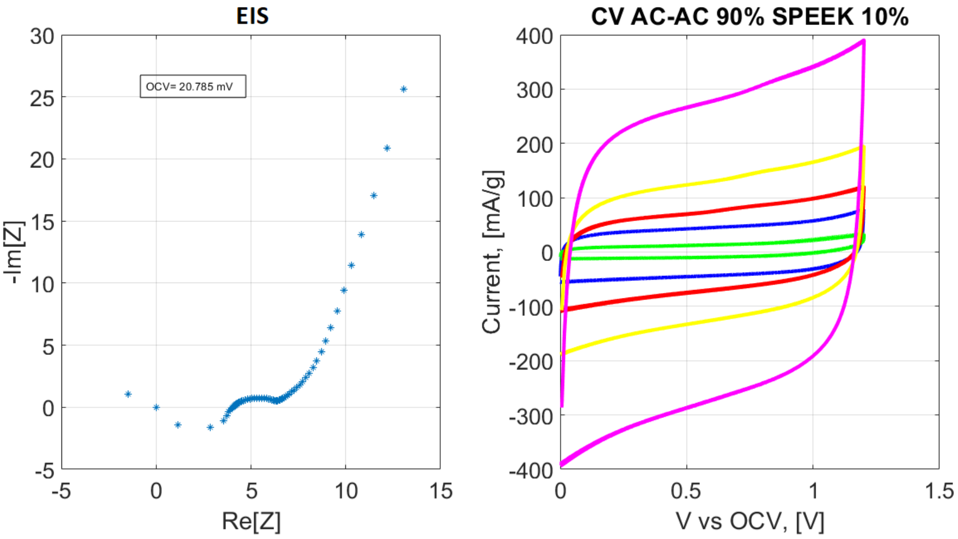

Figure 6.3: Characteristics of AC PVDF - AC 90 % SPEEK 10% device

From impedance spectroscopy, we can notice how the resistance is lower compared to case in figure 6.2: diffusion region is significantly reduced, but the characteristic at low frequencies remains slanting. In CV we have a distortion of the curve which causes a reduction of capacitance, which (evaluated through CCCD) is equal to 9,45 F/g. Efficiency remains stable at 90%.
Following we have the summarize of key parameters.

C [F/g]	ESR [Ω]	τ [s]	E_d [Wh/kg]	P_d [kW/kg]	η [%]
9,45	4,03	0,4642	1,87	7,27	88,5

6.4 AC PVDF - AC 90% SPEEK 10% with infiltrated SPEEK

This attempt is a combination of 2 previous configurations: here we use an activated carbon electrode with PVDF as binder on the anode. On the cathode, we place an activated carbon electrode with SPEEK as binder in 90% - 10% percentage, over which we further infiltrate other SPEEK melted in DMSO.

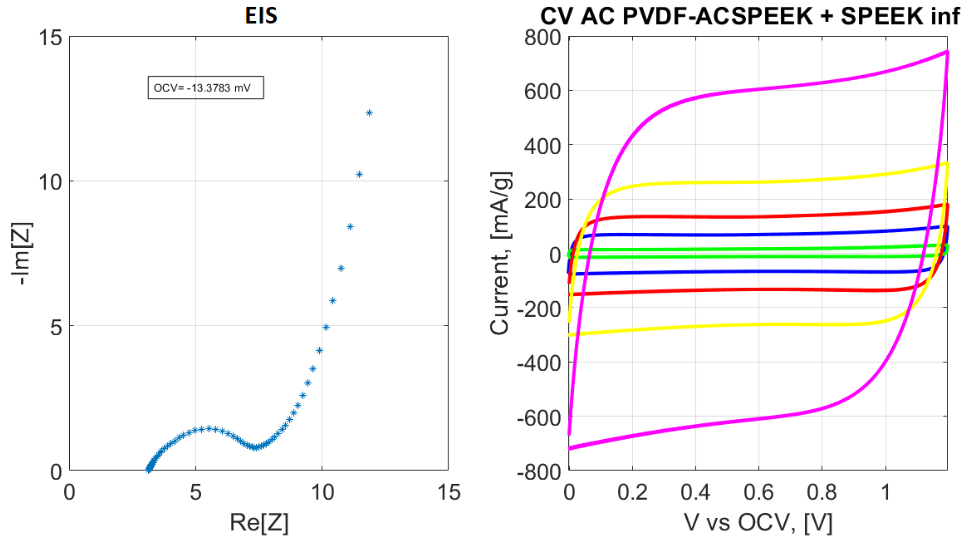

Figure 6.4: Characteristics of AC PVDF - AC 90 % SPEEK 10% with infiltrated SPEEK device

At a first glance we can notice how the CV is much less deformed with respect to the previous cases. For what concerns impedance spectroscopy, we can notice a reduction of the diffusive region we observed in figure 6.3. As advantage, we observe through the CCCD analysis that capacitance value reached is the higher after case in section 6.1. Here we reached 14,57 F/g and an efficiency equal to 88%.
Following we have the summarize of key parameters.

C [F/g]	ESR [Ω]	τ [s]	E_d [Wh/kg]	P_d [kW/kg]	η [%]
14,57	3,11	0,5987	2,894	8,7	87,8

6.5 Synoptic overview

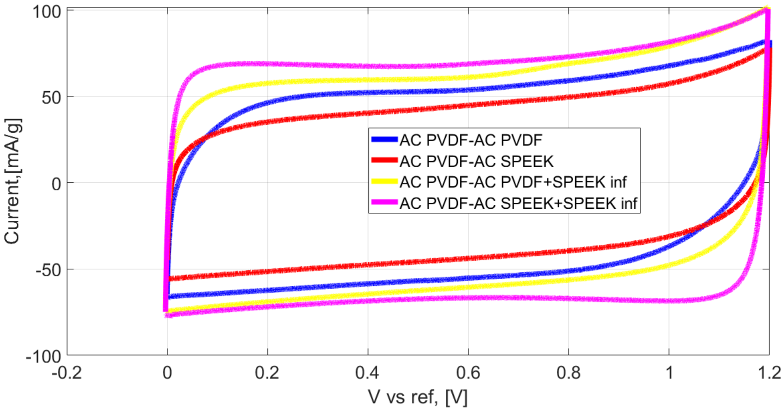

Figure 6.5: CV comparison at 5 mV/s of all configurations.

In figure 6.5, there are represented together all CV curves at 5 mV/s scan rate of all previously presented configurations. So analyzing it, we can tell which is the best configuration among these. Choice appears straight forward: ignoring the blue curve (activated carbons electrodes device on both side), all curves are deformed and not properly squared. The curve most close to a square shape is the pink curve, which is related to configuration exposed in section 6.4, where we have an activated carbon electrode bounded with PVDF and the cathode characterized by SPEEK as binder and as infiltrated membrane over the whole electrode.
In next chapters, we will exploit this configuration in order to try to harvest energy from CO_2 capture with water based electrolytes.

Section	C [F/g]	ESR [Ω]	τ [s]	E_d [Wh/kg]	P_d [kW/kg]	η [%]
6.1	11,9	3.45	0,6786	2,36	6,262	85,2
6.2	12,4	4,87	0,4473	2,45	9,864	89,8
6.3	9,45	4,03	0,4642	1,87	7,27	88,5
6.4	14,57	3,11	0,5987	2,894	8,7	87,8

From tabular above, we can notice how the higher capacitance configuration is the latter one, meaning AC-AC 90% SPEEK 10% with infiltrated SPEEK. Moreover, with this configuration we have also the lower ESR, higher energy density and higher efficiency compared to configuration presented in section 6.1. Also time constant and power density are higher than the uncoated case.

Chapter 7

Preliminary analysis for DABCO IM ionic liquid

From now on, the goal is to translate concepts of chapter 6 from water based electrolytes to ionic liquids. In particular we exploit Diazabicycloundecanium Imidazolide from Iolitec. This liquid is characterized by the combination of a anion (Imidazolide) and a cation (Diazabicycloundecanium): first compound is the anion generated from Imidazole [25], characterized by pentagonal shape. Cation otherwise is again characterized by a ring structure, followed by a chain[]: the whole molecule is overall positively charged, so it is able to remain attached to the anion. Slurry of AC changes, since we change binder and we add carbon black to increase the conductivity, as reported in appendix A.2.

7.1 Setup adopted for ionic liquids electrolytes

Exploiting ionic liquids is not possible to improve a setup similar to the one adopted in water based electrolytes (shown in figure 3.2). In our particular case we used PAT-cells from EL-cell GmbH [26], shown below (figure 7.1).

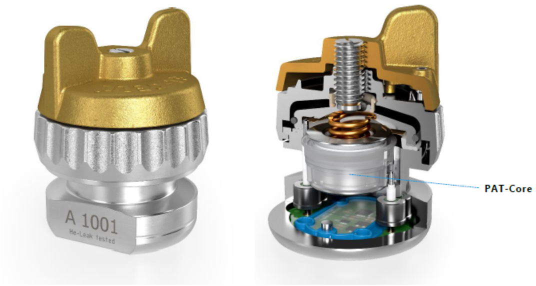

Figure 7.1: Cells adopted from EL-Cell [26]

With this setup we are able to perform both 2 electrodes and 3 electrodes measurements, by properly selecting the suitable PAT-Core. This is formed by 3 principal parts.


(a) (b) (c)

Figure 7.2: Core parts used [27]

Parts 7.2a and 7.2c are called plungers and are used in order to contact electrodes with measurement setup, while part 7.2b is the sleeve and it is used to provide the reference contact, to hold the separator and to avoid short-circuits between top and bottom electrode.

7.2 Selection of the proper separator

In following we will analyze (exploiting a 3 electrodes analysis) behaviour and differences we obtain in CV and EIS using glass fiber and a polymeric separator, using as working electrode the electrodes built following recipe A.2. Used amount of electrolyte is 200 μl for all 3 electrodes measurements.

7.2.1 Glass fiber separator

EL-cell provides a borosilicate glass fiber of 250 μm thickness and high porosity [28]. We place the working electrode on the bottom side of the sleeve and then wet the membrane with about 200 μl of electrolyte. Then we place the counter electrode and wet it too with other 200 μl of electrolyte. Reference is already present in the sleeve. In principle, in this case voltage can rise up over 1,2 V (in modulus) because we have not to pay attention to the water splitting phenomenon.

Already from the cyclic voltammetry in figure 7.3 it is clear that this setup can not be adopted because of the high resistivity of the whole system. Charging and discharging curves are almost overlapped, so we can not say that there is a storage of accumulated charges.

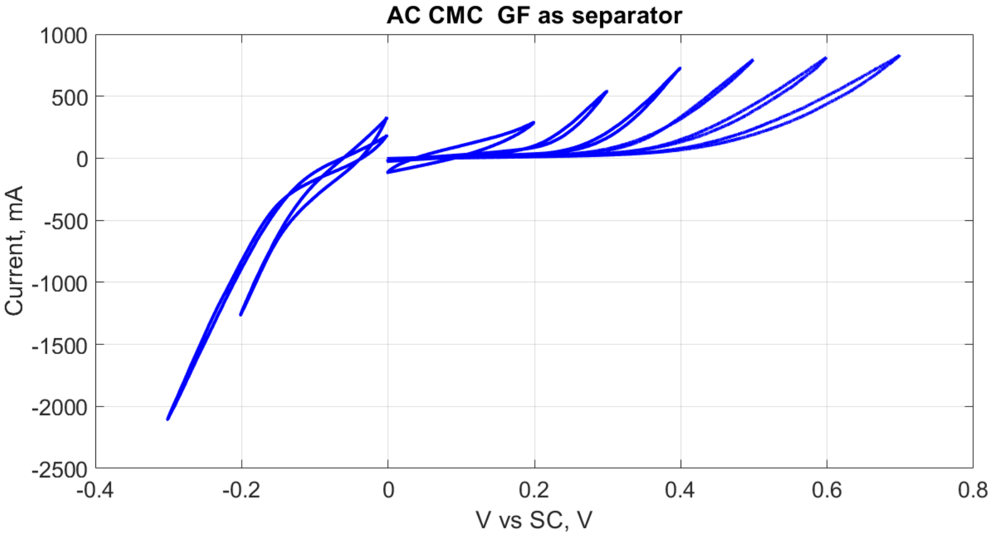

Figure 7.3: Cyclic voltammetry of AC CMC electrode with glass fiber as separator

Moreover we cannot evaluate if the electrolyte has a region in which shows better performances avoiding degradation.

7.2.2 Polymeric separator: FS2226

This separator is formed by PE fiber/PE membrane [27]. In EL-cell GmbH catalogue this membrane shows a middle level of porosity (67%, much lower than glass fiber) and a good wettability.
Also in this case, procedures for electrode installation is the same of the one described in section 7.2.1, with AC CMC electrode as working and a carbon pill as the counter. Total electrolyte amount is still 400 μl, in order to properly wet the counter electrode.

Already here in figure 7.4, we can notice how the potential window is much larger compared to water based electrolytes, since we can reach -1,3 V and +0,3 V maintaining Coulombic efficiency over 95%, and capacitances up to 40 F/g. Drawback is ESR value (over 25 Ω) and the shape of the Nyquist plot which at low frequencies shows a great dependence of impedance from working frequency. These characteristics are mainly due to the nature if the ionic liquid which ensures an higher value of potential window compared to water based devices, but increases also the equivalent series resistance because of the high viscosity of the liquid.
Concluding this section, between our two possible separators, the best one is surely the polymeric one. From now on all our measurements are performed with this membrane.

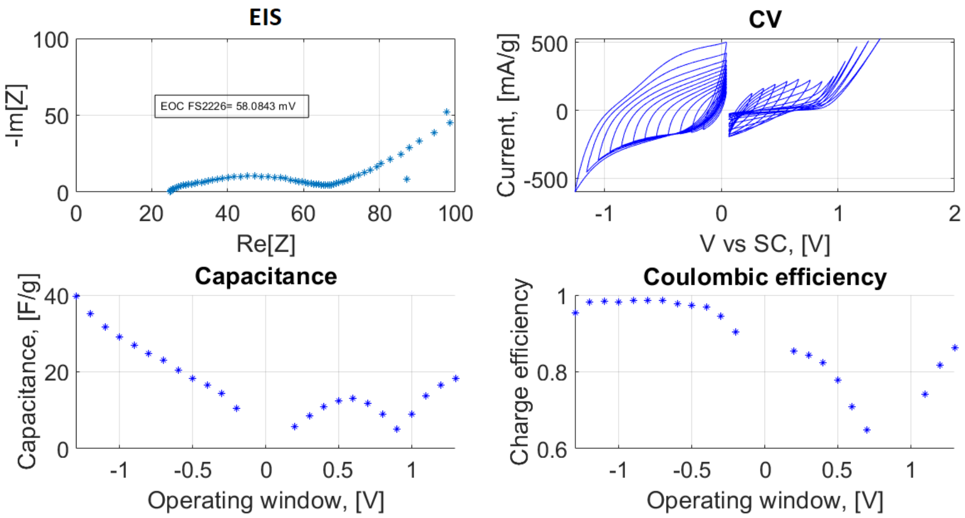

Figure 7.4: Characteristics of AC CMC electrode with polymeric separator

7.3 Gas diffusion layer

In order to allow the propagation of gas inside the sealed cell, we can exploit a gas diffusion layer (GDL). GDL can be used as electrode, since it is generally a carbon paper, characterized by high porosity, able to guarantee air permeation [29, 30]. Moreover it has to avoid liquid diffusion through it. In our case thickness of GDL is 250 μm.

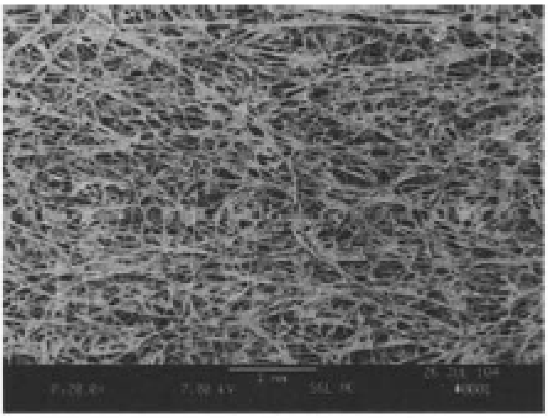

Figure 7.5: Scanning electron microscope acquisition of GDL surface [29]

Here we perform the same 3 electrodes analysis made before with activated carbon electrodes in order to select the better way to place electrodes: which one shows better performances in positive or negative polarization.

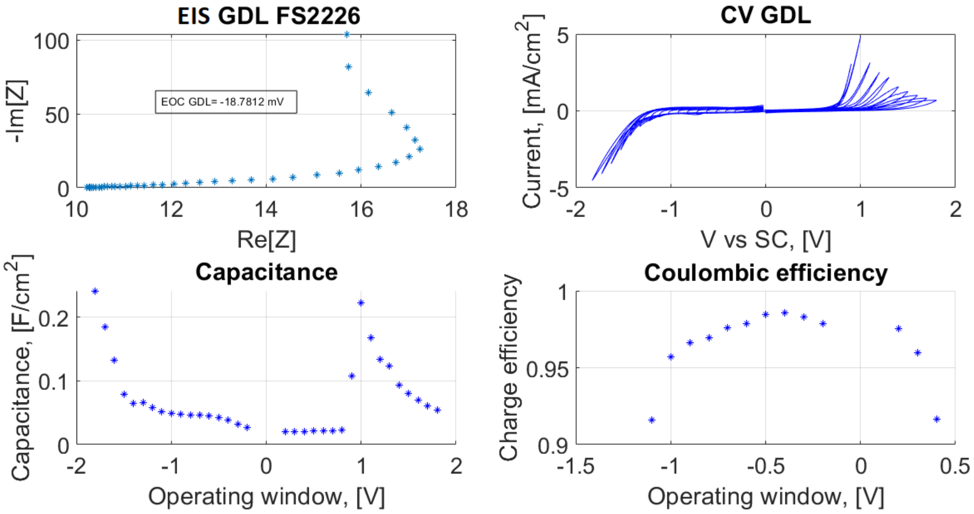

Figure 7.6: Characteristics of GDL electrode

In this case, the normalization is respect the surface area, since it is not clear the real amount of carbon inside the GDL, so it is hard to know its mass. Anyway, conclusion we can make about gas diffusion layer (exploiting figure 7.6) are that we can use it, guaranteeing an efficiency greater than 95% from -1 V to +0,3 V. Resistance is half of the value obtained with activated carbons and, except for a quite wide diffusive region, we have a good stability of resistance with the frequency at low frequencies.

7.4 Cell configuration

Now we have to define how to build the cell we will then test in presence of CO_2. First thing to do is to evaluate which electrode place on the positive electrode and which on the negative one. Firstly we analyze charge efficiency and capacitances vs applied potential (figure 7.7). Here, for 2 electrodes measurements, we use 100 μl of electrolyte.

In figure 7.7, all measurements are related to the surface area of electrodes, since as previously explained we are not able to state anything sure about the GDL mass, so we decided to make all our considerations reported to surface. What we can clearly say is that we have better performances in negative polarization for both electrodes. Voltage at which polarize the system is evaluated considering the

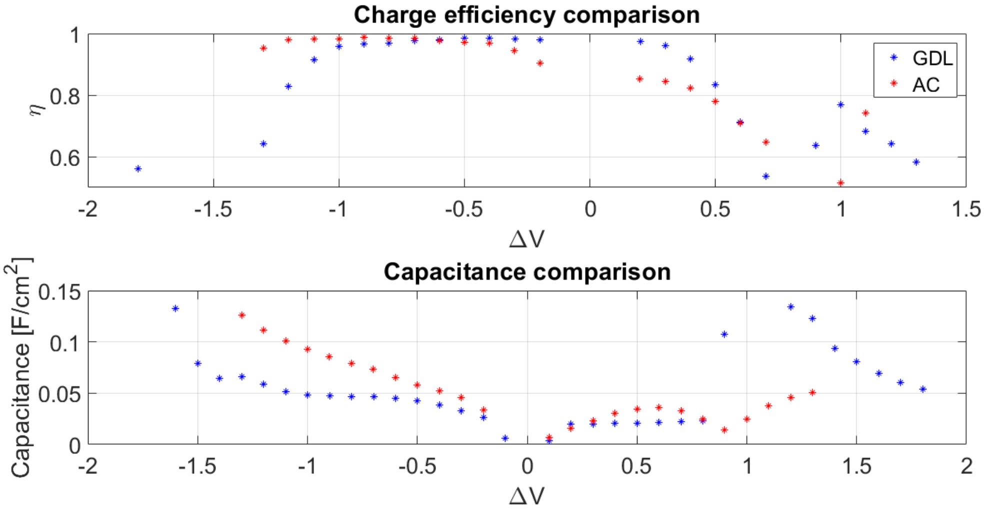

Figure 7.7: Comparison of charge efficiency and capacitance/cm^2 of AC and GDL

maximum voltage at which we have a charge efficiency grater than 95%: data are reported in the following table.

	Negative		Positive	
	V [V]	C [mF/cm^2]	V [V]	C [mF/cm^2]
AC	-1,2	116	0	0
GDL	-1	24	0,3	10

We can have 2 possible choices: AC on the cathode and GDL on anode, or GDL on both sides. At this point, since we have so different capacitances at both electrodes of the cell, we have to make them similar playing of the ratio of their surfaces: if we do not act in this way, we can notice that charging of anode and cathode happens with different constant of time, which can lead to a malfunctioning of the device, as depicted in figure below 7.8.

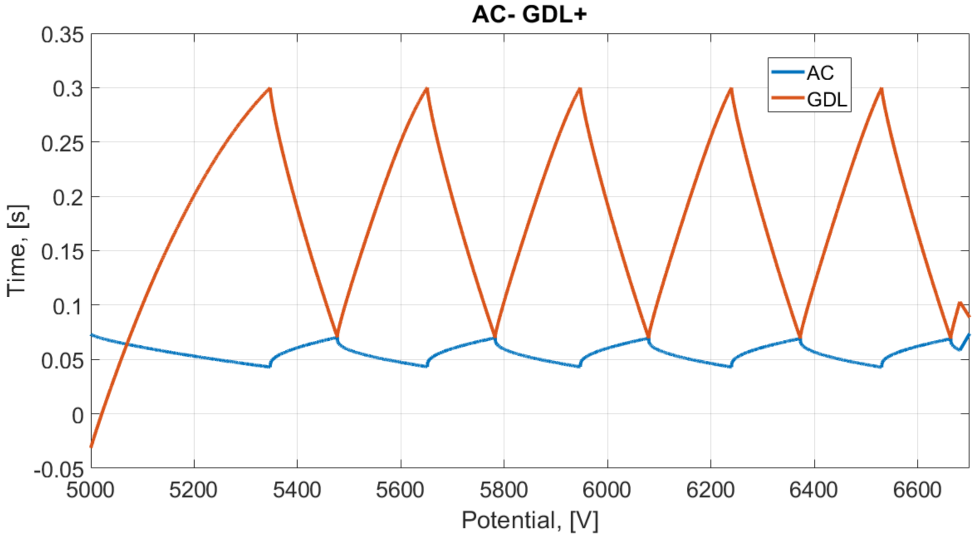

Figure 7.8: CCCD at 0,1 mA/cm^2 of cell with AC on cathode and GDL on anode

In figure 7.8, we would polarize AC at -1,2 V and GDL at +0,3 V at the same time. This clearly does not happens and we are able to completely charge only GDL, whereas AC does not reach its imposed threshold. Moreover in order to maximize the total capacitance value of the cell, we have to engineer electrodes to make them of the same capacitance. We can solve these issues just applying the formula:

$$\Sigma_{AN} C_{AN} = \Sigma_{CAT} C_{CAT} \tag{7.1}$$

Where Σ_{AN} and Σ_{CAT} are surface of anode and cathode and C is the associated capacitance. Developing all calculations for the 2 possible configurations (meaning activated carbon on cathode and gas diffusion layer on the anode, or GDL on both sides) we get: We also needed to prevent contact between steel of the cell and electrolyte in order to avoid unwanted reactions. Performing a rapid CV measurement at 0,5 V (widely inside the operating window) exploiting the so evaluated electrode measurements, we can observe the effect of interaction between the electrolyte and the steel of the cell compared to the CV of a correctly insulated cell.

AC- GDL+		GDL- GDL+	
V_-= -1,2 V	V_+= 0,3 V	V_-= -1 V	V_+= 0,3 V
C_-= 116 mF/cm^2	C_+= 10 mF/cm^2	C_-= 24 mF/cm^2	C_+= 10 mF/cm^2
$\frac{\Sigma_+}{\Sigma_-}$= 11,6		$\frac{\Sigma_+}{\Sigma_-}$= 2,4	
Σ_-= 21,94 mm^2	Σ_+= 254 mm^2	Σ_-= 106 mm^2	Σ_+= 254 mm^2
d_-= 5,2 mm $\Rightarrow$ 5 mm	d_+= 18 mm	d_-= 11,6 mm $\Rightarrow$ 12 mm	d_+= 18 mm

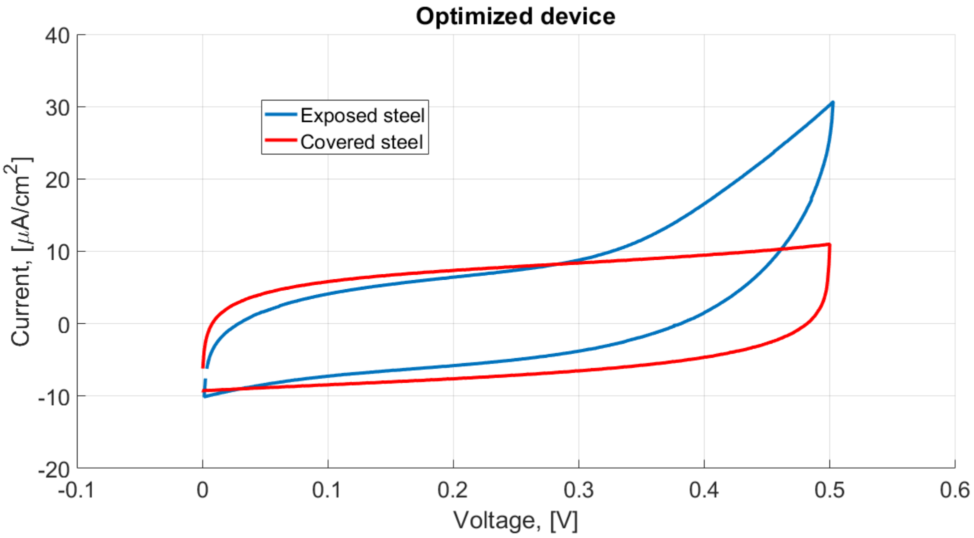

Figure 7.9: CV from 0 V to 0,5 V of optimized cell, in order to evaluate the steel-electrolyte interaction

Now, measurements we can perform are constant current charge discharge evaluation, in order to evaluate the way both electrodes are charging themselves when we polarize the system. The measurements are performed in unbalanced cells. Then, the last measure is the leakage current and self discharge, which is the procedure to implement when we will then flux CO_2.

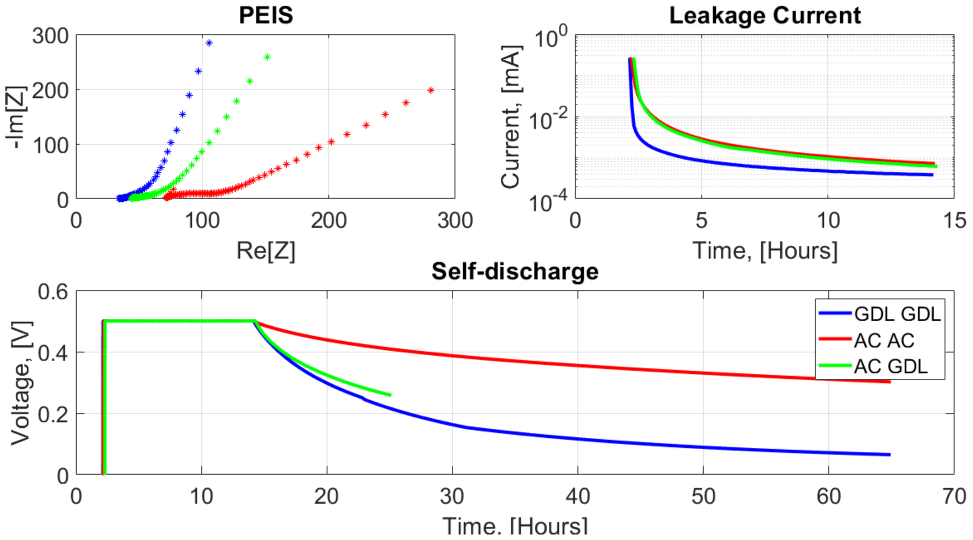

Figure 7.10: Leakage current and self discharge analysis for 3 configurations with 18 mm diameter electrodes

In this procedure we charge at a constant current (0,1 mA/g) until reach 0,5 V. At this point we hold that tension and measure the leakage current. When we reach 0 A (or almost a negligible current), we release the voltage and measure the self discharge rate. In figure 7.10, we can observe how the AC-AC device is the slower releasing voltage device, while GDL-GDL is the faster one. It is interesting to notice that the AC-GDL device is a trade off between both previous configurations.
This procedure has to be implemented also in gas evaluations.

Chapter 8

CO_2 measurements in ionic liquid

In this section, we will analyze what happens when we flux CO_2 inside the device studied in the previous chapter. Finally we opted for a device made by 18 mm diameter GDL for anode and 12 mm diameter GDL for cathode. The choice was due both to the easier assembling and because in this way it would be possible in the future to flux gas from both side of device.

8.1 Procedure

The procedure adopted can be divided in 4 steps shown in figure 8.1.

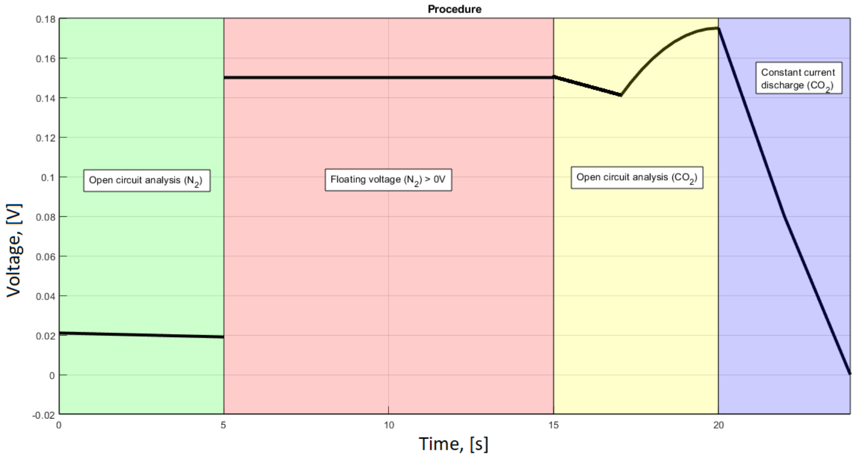

Figure 8.1: Schematic of the procedure

First of all, we perform a CV before each test, in order to ensure the stability of the system and the absence of any kind of reaction peaks, as done in figure 7.9.

Making reference to figure 8.1, steps we have to follow are:

- Open circuit analysis (green shaded area): during first cycle, this open circuit has to be done in absence of gas, in order to obtain a figure of merit of the natural OCV of the unperturbed cell, from second cycle in this step we will flux N_2 in order to regenerate the electrolyte.

- Floating voltage (pink shaded area): here we hold for a setted time (generally 10 minutes) a fixed voltage (50 mV, 150 mV, 250 mV 500 mV). Again: for first cycle, we do not flux anything, for following cycles we flux N_2. In this step, we have also to monitor the current and ensure that this decreases to 0 A in exponential way.

- Open circuit analysis (yellow shaded area): here we stop the hold potential and switch on the CO_2 flux. We measure how the gas affects the open circuit voltage: we expect to see a rise in the voltage, or at least a reduction in self-discharge decrease.

- Constant current discharge (blue shaded area): once reached the maximum due to the electrolyte absorption of CO_2, we can discharge the device through a constant current until reaching 0 V. Then we can restart the process from first step (green shaded area), opening N_2 flux.

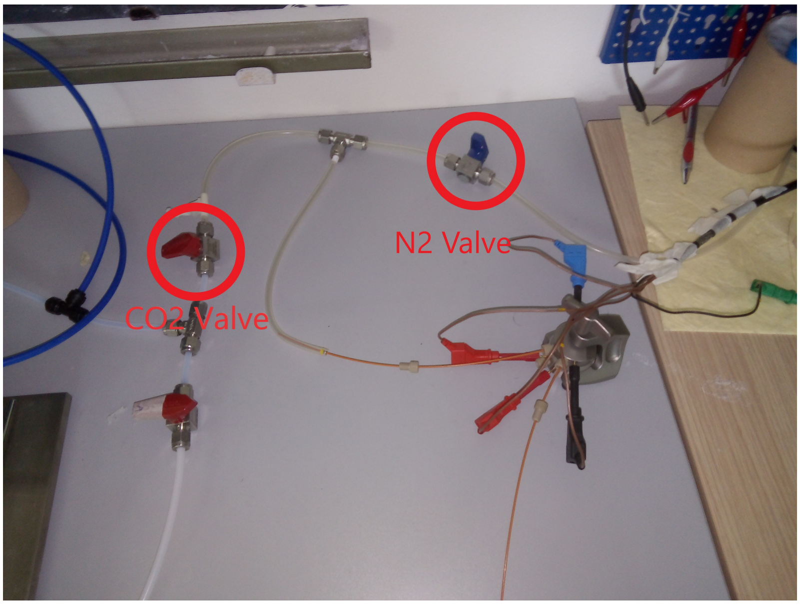

Figure 8.2: Setup adopted for CO_2 capturing evaluation

In principle this procedure has to work also for a float potential equal to 0 V, however, setting an higher potential, we are able to fix the amount of charges we provide to the system and make the measure reproducible, avoiding any possible drift due to uncontrollable parameters (such as temperature) and minimizing leakages.

8.2 50 mV floating

As explained in section 7.4, we have two different electrodes diameter. Configuration adopted is reported in figure 8.3.

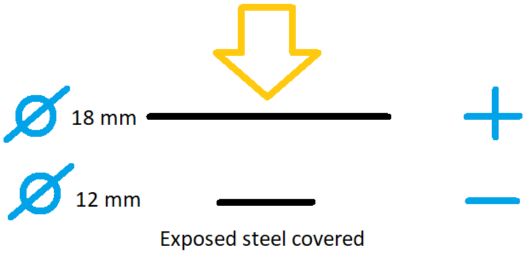

Figure 8.3: Electrodes configuration and direction of the gas flux

We placed positive contact at the larger electrode and negative contact to the smaller one. Gas is flushed through the positive electrode. Negative steel contact has been covered with Kapton in order to prevent reactions with the electrolyte.

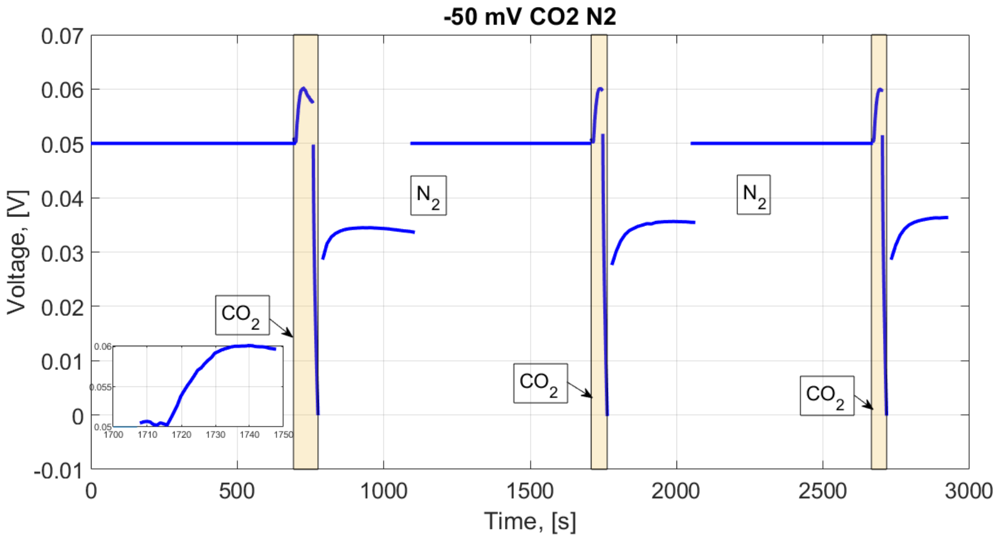

Figure 8.4: Evaluation of voltage gain due to CO_2 flux

Holding 50 mV of floating voltage and flushing CO_2, we have a good repetibility of the gain, which is around 10 mV (gain of 20% compared to floating voltage) for each repetition. Before each float and each float itself, we flux inside the device N_2 gas, in order to regenerate the electrolyte. Regeneration works pretty well, since at each open circuit voltage analysis after constant current discharge, the device fastly reaches the same stable OCV, around 35 mV.
In discharge curve, the first choice (which regarded all this test) was to fix the current at 10 μA/cm^2. However we noticed an important IR drop, so for the following measurements we decided to reduce the current rate to 1 μA/cm^2.

8.3 150 mV floating

Here we fluxed gas through the negative electrode, which now is placed on the top of the chamber, as depicted in figure 8.5. Also in this case we paid attention in insulating steel of the setup from electrolyte inside the super-cap.

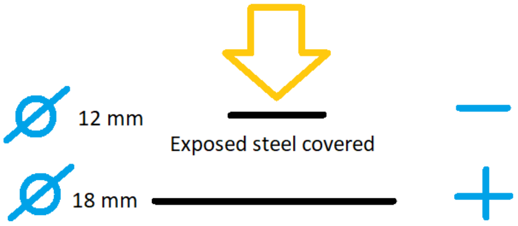

Figure 8.5: Electrodes configuration and direction of the gas flux

During this analysis we did not performed regeneration trough N_2, but we were more interested in thermal regeneration.

In figure 8.6, we can notice in the first and second CO_2 flux a gain greater than 20 mV (gain of 13% compared to floating voltage) and a correct constant current discharge (performed at 1 μA/cm^2), which allows us to perform some energetic evaluations. In OCV recordings before floating, we can observe how the adsorbed CO_2 affects the open circuit voltage of the cell, which now does not reaches in a fast way the same stable value reached in section 8.2, but increases. This is due to the lack of N_2 regeneration step. At the third flux of CO_2, we can clearly see how the gain in the voltage is low, because electrolyte becomes near to the saturation.
We can make some energetic evaluations comparing the energy needed to charge the device(E_c), energy spent in holding the floating voltage (E_f) and the discharge energy (E_d). Difference between E_d and E_f is the net energetic gain we obtain in this configuration with this procedure, while difference between E_d and E_c is the

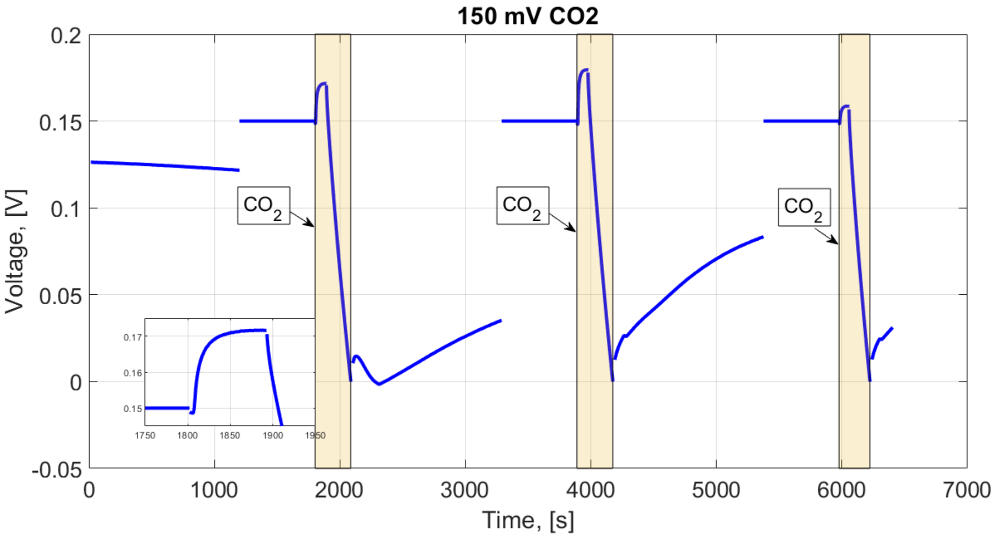

Figure 8.6: Evaluation of voltage gain due to CO_2 flux

maximum energy we can gain. Moreover is reported also the average discharge power ($< P >_d$), in order to be able to place correctly our device inside a Ragone plot.

Formulas used in order to evaluate energies are the following:

$$E_c = \frac{1}{2}CV^2 \quad , \quad E_f = \int_{t_{float}} VI\ dt \quad , \quad E_{CCD} = \int_{t_{CCD}} VI\ dt \tag{8.1}$$

$$\Delta t_c = \frac{\Delta t_d}{\eta_{Coulombic}} \quad , \quad < P >_c = \frac{E_c}{\Delta t_c} \quad , \quad < P >_{CCD} = \frac{E_{CCD}}{\Delta t_{CCD}} \tag{8.2}$$

In previous formulas we have E_c and $< P >_c$ charge energy and power, C capacitance, V polarization voltage, E_f and $< P >_f$ floating energy and power, E_{CCD} and $< P >_{CCD}$ constant current discharge and power, $\Delta t_{c/d}$ charging/discharging time. We have $\eta_{Coulombic}$ Coulombic efficiency equal to 87% and C capacitance equal to 346,25 $\mu F/cm^2$, both evaluated from CV at 150 mV. Results are reported in table below. Δ t_d is the time needed to reach 0V from 150 mV in constant current discharge, while Δ t_{CCD} is the total time in constant current discharge.

	E_c $[\frac{nWh}{cm^2}]$	<P>$_c$ $[\frac{mW}{m^2}]$	E_f $[\frac{nWh}{cm^2}]$	<P>$_f$ $[\frac{mW}{m^2}]$	E_{CCD} $[\frac{nWh}{cm^2}]$	<P>$_{CCD}$ $[\frac{mW}{m^2}]$
I	1,08	0,1869	1,15	0,069	4,06	0,753
II	1,08	0,1887	3,63	0,2178	4,34	0,7893
III	1,08	0,2014	3,62	0,2172	3,21	0,6918

Where I, II, III are the n$-th$ cycle. Also from here we can observe how E_d at third cycle significantly decreases compared to the previous cycles.

Comparing E_c and E_f columns, it is evident how the floating energy is much higher than the energy actually needed to charge the capacitor. We chose to maintain for 10 minutes the floating voltage in order to be sure to minimize leakages. Reducing floating time, energetic gain can be higher. It has also to be kept in mind that between each cycle we did not regenerated with N_2.
In following table, are reported some other energetic considerations.

	E_{CCD}-E_f $[\frac{nWh}{cm^2}]$	E_{CCD}-E_c $[\frac{nWh}{cm^2}]$	$\frac{E_{CCD}}{E_f}$	$\frac{E_{CCD}}{E_c}$	$\frac{E_{CCD}-E_f}{E_f}$	$\frac{E_{CCD}-E_c}{E_c}$	CO_2PCE_{ex}	CO_2PCE_{th}
I	2,91	2,98	3,53	3,75	2,53	2,75	10,91	4,03
II	0,71	3,26	1,19	4,02	0,196	0,657	3,62	4,18
III	-0,41	2,13	0,88	2,97	-0,11	1,97	3,18	3,43

Factors CO_2PCE_{ex} and CO_2PCE_{th} are CO_2 induced power conversion efficiency through experimental (evaluated as $< P >_{CCD}/< P >_f$) and theoretical evaluation (evaluated as $< P >_{CCD}/< P >_c$). In the table above all parameters are related to the I cycle, in which we do not already have effect of saturation and the cell is not already conditioned by CO_2 absorption. We have in first, third and fifth column respectively the energetic gain (in modulus), total energetic efficiency and relative energetic efficiency all related to experimental values, while in second, fourth and sixth column we have the same values related to the theoretical maximum extractable charge. In the first cycle, we have $P_{CCD}/P_c < P_{CCD}/P_f$ because we start to charge the device from a very high OCV (120 mV) as shown in figure 8.6, while P_c considers the charge from 0 V. In third cycle we have $E_{CCD} - E_f < 0$: this means that the energy needed to hold the float is too high to recover energy. In fact we have theoretically an energetic efficiency greater than 1, but the experimental one is smaller. Reduction in power efficiency is one of the effects of the undone regeneration of the electrolyte.
E_c id the energy related to the hypothesis we charge the device at 150 mV with a constant current equal to 1 μA/cm^2 providing to it 1,08 nWh/cm^2 in Δt=206 s (conditions to charge completely the device at 150 mV and not have losses due to the holding of floating voltage). In general, efficiencies are greater than one, but this is due to the fact that we have a gain due to the flux of CO_2 after floating, which generates a gain. Moreover we are neglecting all the energy needed to store CO_2 inside the cylinder and the energy needed to flux it inside our device. Experimental energies and efficiencies are lower than the theoretical one because of the too long floating voltage holding, which causes the dissipation of energy in holding voltage at 150 mV.

After these cycles of measurements, we thermally regenerated the device at 80° C for 1 hour and then we repeated the CO_2 measurements.
In figure 8.7 we can see how the thermal regeneration took back the electrolyte to

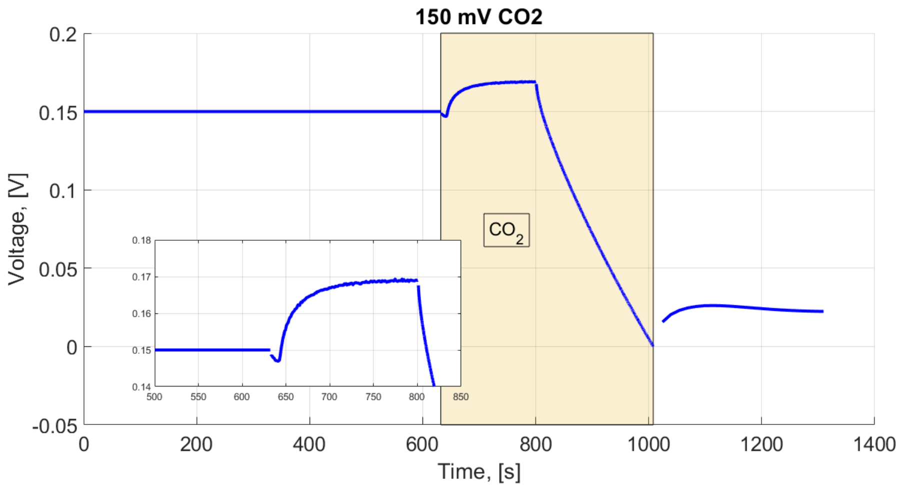

Figure 8.7: Gain due to CO_2 after thermal regeneration

initial conditions, where we were able to gain again 20 mV (gain of 13% compared to floating voltage).

8.4 250 mV floating

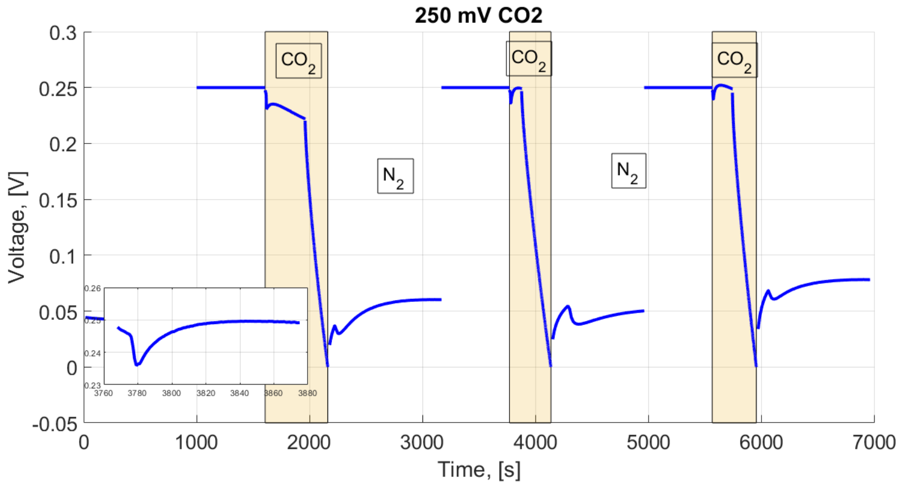

Figure 8.8: Gain due to CO_2 after floating of 250 mV

Configuration adopted is the same of figure 8.5. In figure 8.8 we can observe how we have no gain over the floating voltage: when we switch off the holding voltage, we have a initial decrease of voltage equal to 15 mV and a subsequent gain of the same amount. This will not translate in a general gain of energy, so this floating voltage is clearly too high to harvest energy from CO_2 capture.

8.5 500 mV floating

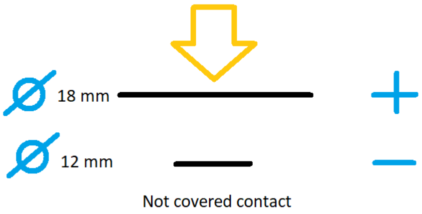

Figure 8.9: Electrodes configuration and direction of the gas flux

This voltage was definitely much higher compared to the previous one, however this was the only case in which we could use a flowmeter, and the result was pretty interesting.
Configuration is shown in figure 8.9, and the steel of the cell was exposed (not the best operating condition), however we get the following curve 8.10.

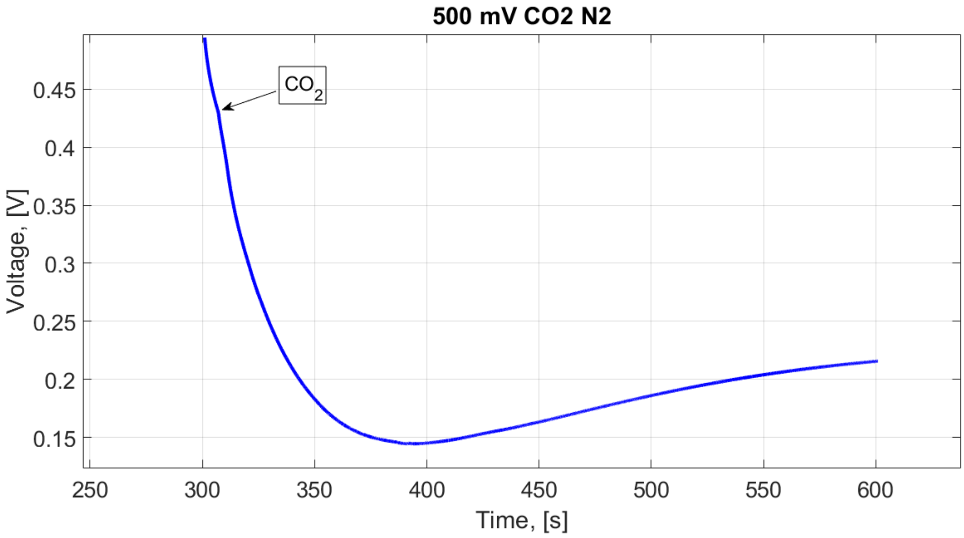

Figure 8.10: Gain due to CO_2 after floating of 500 mV

After an important decrease from 500 mV to 150 mV, we can observe the contribution of CO_2 absorption: once reached the minimum, voltage starts again to increase, gaining more than 50 mV. According to this only measurement, pressure might be a key parameter to be controlled as the gain was much higher.

8.6 Symmetric electrodes

Last experiment performed was realized in order to ensure if electrodes optimization was really effective on our measurements. We decided to reproduce 150 mV floating measurements in order to compare the CO_2 gain between asymmetric device and symmetric device. Considering figure 8.7 as figure of merit, the following is new curve.

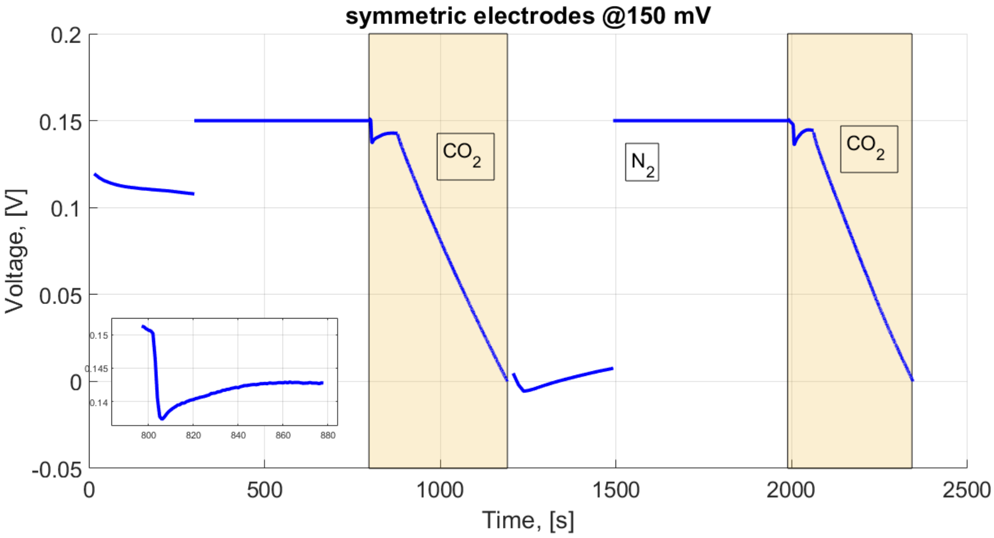

Figure 8.11: Gain due to CO_2 after floating of 150 mV in symmetric device

We observe in figure 8.11 the same behaviour observed in figure 8.8: we have a gain in voltage, but only after a steep voltage decrease. This can mean that using symmetric electrodes we have a limitation of the voltage window at which we can polarize our device and 150 mV is already out from that voltage window.

Chapter 9

Conclusions and future developments

9.1 Selection of membrane and binder in water electrolyte

In water based electrolyte, we performed some measurements with different infiltrated membranes, both anionic and cationic. However only cationic one were properly produced and can be used. In particular the best one was sulphonated poly-ether ehter ketone (SPEEK).

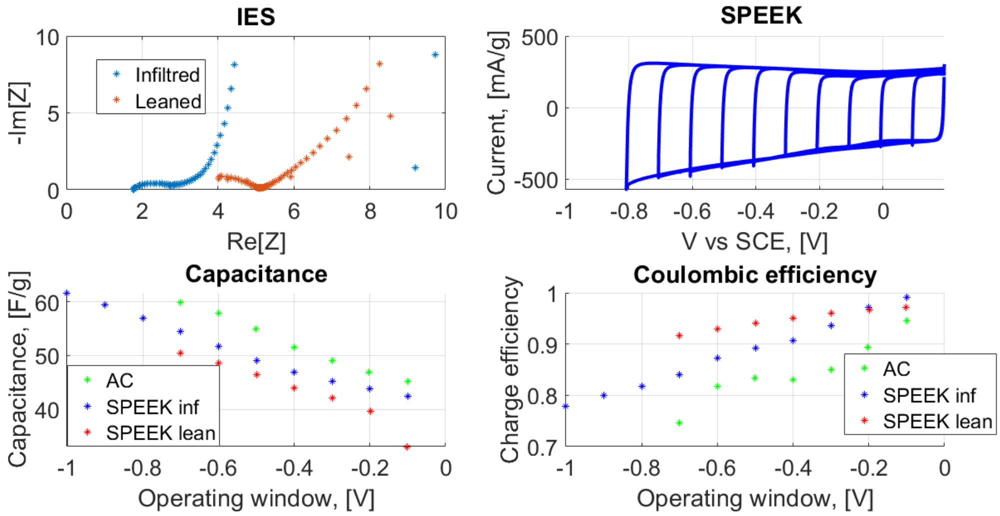

Figure 9.1: SPEEK membrane analysis

Compared to pure activated carbons of figure 4.4, here we have a reduction in

capacitance from 60 F/g to 55 F/g, we notice an improvement in charge efficiency and we have no increase of ESR (lower graphs in figure 9.1). Comparing infiltrated membrane analysis to leaned membrane, we can notice how capacitance is increased with infiltration and internal resistance is strongly reduced. We pay in terms of efficiency, since in leaned membrane device we have the higher values.
Another idea arose in order to reduce ESR, was to substitute PVDF (binder adopted in activated carbons slurry) directly with SPEEK. Selected percentage was AC 90% SPEEK 10%. Measurements are presented in figure 9.2 .

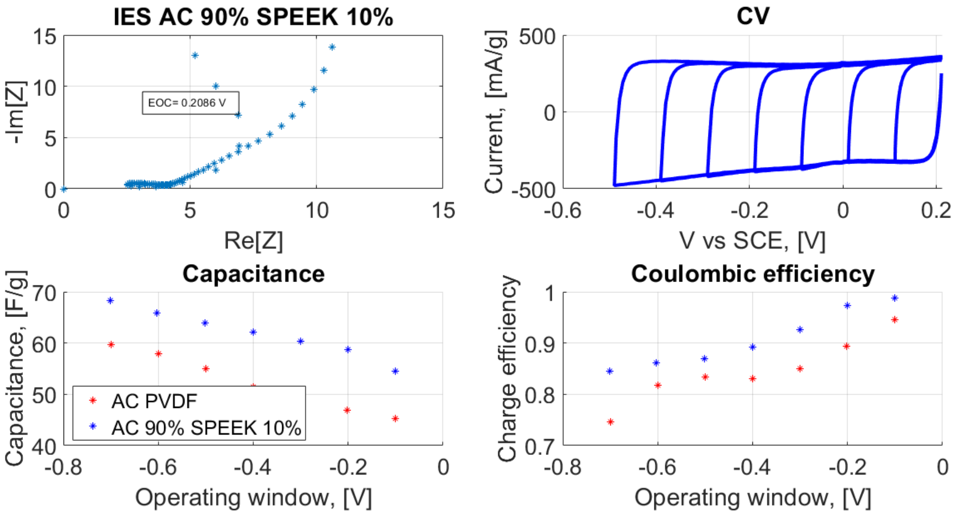

Figure 9.2: AC 90% SPEEK 10%

9.2 Ionic liquid

In ionic liquids we worked in a device which exploited Diazabicycloundecanium Imidazolide as electrolyte and the first issue was to find a good separator for the electrolyte: we tested basically 2 separators (glass fiber and a polymeric separator, in particular PE fiber/PE membrane: FS2226 from EL-cell GmbH). Polymeric membrane resulted to be the better one.

Then we proceeded to an analysis related to gas diffusion layers, which are needed in order to let a gas flux flowing inside the cell of measurements. As we can immediately see also from figure 9.3, capacitances values are not the same for anodic and cathodic analysis: this means that we need to optimize electrodes in order to obtain charge at the maximum capacitance of both sides in the same time. This can be done exploiting formula 7.1. This formula ensures also the fact that the capacitance of both electrodes is the same, so the overall capacitance is maximized.

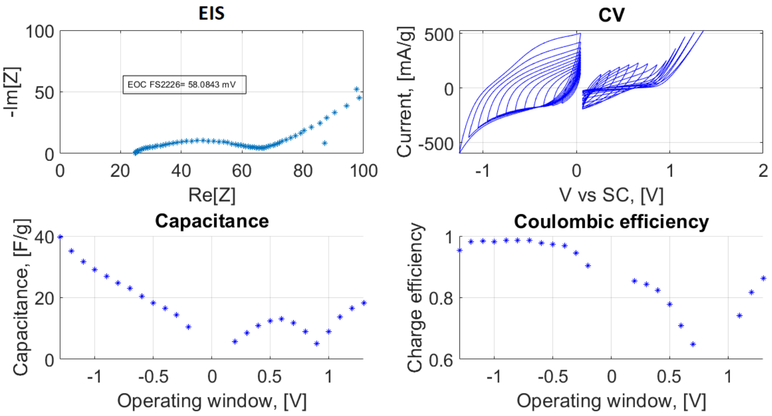

Figure 9.3: Characteristics of AC CMC electrode with polymeric separator

After several considerations, we decided that the best configuration is the one with 2 GDL: anode with 18 mm diameter, cathode with 12 mm diameter. This allows us to reduce complexity in assembling phase and to have future possibility to flux gas both from anode and from cathode.
With this configuration we proceeded to measurements in CO_2.

9.3 CO_2 measurements in ionic liquid

Best results where achieved for 50 mV float and 150 mV in which with asymmetric devices we are able to reach voltages grater than floating voltages.

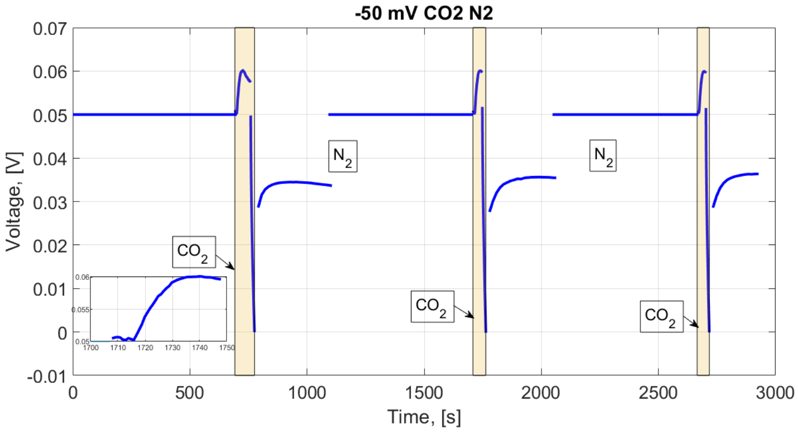

Figure 9.4: Evaluation of voltage gain due to CO_2 flux

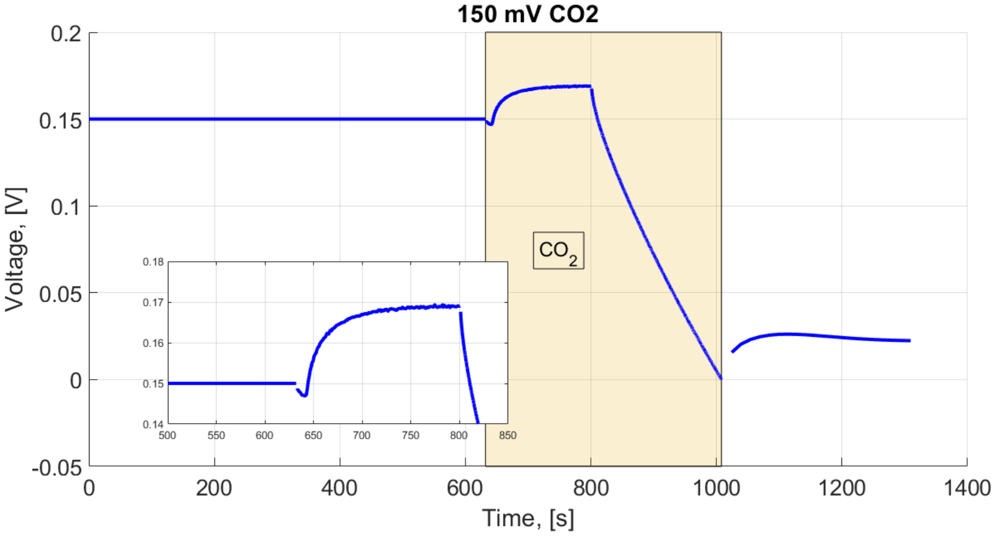

Figure 9.5: Gain due to CO_2 after thermal regeneration

With 50 mV of float (figure 9.4), we can reach 20% gain compared to the floating voltage, which is equal to 10 mV, while with 150 mV float (figure 9.5) we have a gain of 13%, equal to roughly 20 mV. Moreover for 150 mV floating voltage, temeperature regeneration was proven to be effective to recover IL performances: after 1 hour at 80° C electrolyte is free of CO_2 and ready to absorb new CO_2.

9.4 Future developments

In future we can perform similar tests presented in chapter 8 also for aqueous electrolyte devices exploiting membrane modified electrodes with infiltration and compare them with literature results. Also in aqueous electrolyte, define a good anionic exchange membrane as done for cationic exchange membranes.

In ionic liquid devices, we can evaluate the effect of gas pressure with respect to the absorption of the electrolyte and try to build a cell in which we can flux CO_2 from the cathode and N_2 from the anode: in this way the idea is to favour with the gas flux the motion of cation in place of anion, depending on gas fluxed and direction of the flux.

Other developments can be the following:

- test optimized activated carbon with optimized membranes in ionic liquids electrolyte flushing CO_2
- test the device without any floating voltage, but exploiting only the voltage gain coming from Donnan potential

- test other electrolytes for CO_2 capture as electrolytes and test Dyazabicicloundecanium Imidazolide in solution with other solvents in order to reduce viscosity of the electrolyte itself
- test vacuum instead of N_2 flux in order to induce CO_2 desorption, applying pressure-swing principles
- define in more accurate way measurement protocol of energy harvesting from CO_2 in terms of interval of time, temperature and pressure
- Project and optimize a dedicated cell only for this kind of purposes

Appendix A

Recipes

A.1 AC slurry for water based electrolytes

Composition:

- 90% *wt* Active carbons (AC)
- 10% *wt* Poly-vinylidene fluoride (PVDF)
- Dimethyl sulfoxide (DMSO) as solvent (1 mL/10 mg of binder)

First of all we put the solvent (DMSO) in a becker and add PVDF, which acts as binder. If PVDF does not dissolves in the solvent using stirring, it is suggested to sonicate the solution at 59 KHz for about 30 minutes. Once binder is dissolved, we gradually add active carbons while stirring the solution. For a more uniform dispersion, could be useful to heat the slurry up to 50°C, covering the becker in order to prevent evaporation of the solvent and drying of the slurry itself. Heating and stirring must be carried on for a couple of hours.

In order to spread the slurry over a Ti collector (washed with a solution of distilled water, ethanol and acetone), we exploit a spatula paying attention to have a uniform covering of titanium. If we gently press with spatula on the border of collector while spreading slurry, I found the result is more uniform and compact. Once the layer of AC is on Ti, we have to dry it using a heating plate at 60°C for few minutes: this allows to have a gradual dry of the slurry without generating cracks on the electrode.

A.2 AC slurry for ionic liquids electrolytes

Composition:

- 85% *wt* Active carbons (AC)
- 10% *wt* Carbon black (CB)
- 5% *wt* Carboxy-methyl cellulose (CMC)
- Demineralized water as solvent (1 mL/10 mg of binder)

Basic indications are the same reported in A.1 for the binder (in this case CMC). Carbon black is a finer type of active carbons: they are used in order to reduce resistance. CB generates conductive filaments among AC grains.

In this case collector is an aluminium foil washed with solution of ethanol and acetone. This foil is placed on a glass, and to guarantee an optimal attachment, we spray some drops of acetone over the glass. Al is hold still through a claw and the slurry is spread with a sort of iron rolling pin generating a uniform coating. Then the foil is dried in oven at 40°C for about 1 hour.

A.3 Counter electrodes pills

Composition:

- 85% *wt* Active carbon (AC)
- 10% *wt* Poly-tetrafluoro ethylene (PTFE)
- 5% *wt* Carbon black (CB)
- Ethanol as solvent (2 mL/mg of total weight)

Once properly mixed all the components (where PTFE is the binder), we let stir at 70°C the solution in order to evaporate the solvent until reaching a composite with a consistency similar to the clay. Then it is possible to handle the paste and rolling it out. Finally using a punch (punzone) we cut electrodes in pills that can be dried in oven at 100°C.

For water based electrolytes it is possible to directly insert Ti collectors inside the pills, while for ionic liquids it is not requested any other processing.

A.4 AC SPEEK slurry for water based electrolytes

A.4.1 90% AC 10% SPEEK

- 90% *wt* Active carbons (AC)
- 10% *wt* Sulfonated poly-ether ehter ketone (SPEEK)
- Dimethyl sulfoxide (DMSO) as solvent (in order to melt SPEEK in 40 mg/mL)

First of all, we melt SPEEK in DMSO in order to achieve the concentration of 40 mg/mL. Once we have the correct concentration, we add active carbons and we leave the solution stirring for a couple of hours at 60°C in a closed vial, in order to correctly mix all compounds together. The obtained solution can be deposed on a Ti electrode using a pipe (the solution is very liquid). We have to proceed to a couple of depositions in order to obtain an homogeneous coating of the collector.

A.4.2 70% AC 30% SPEEK

- 70% *wt* Active carbons (AC)
- 30% *wt* Sulfonated poly-ether ehter ketone (SPEEK)
- Dimethyl sulfoxide (DMSO) as solvent (in order to melt SPEEK in 40 mg/mL)

Operations to do are the same of 90% AC 10% SPEEK composition.

Bibliography

[1] European Commission, "Causes of climate change — Climate Action," 2018. [Online]. Available: https://ec.europa.eu/clima/change/causes{_}en

[2] B. E. Logan and M. Elimelech, "Membrane-based processes for sustainable power generation using water," *Nature*, vol. 488, no. 7411, pp. 313–319, 2012.

[3] H. V. Hamelers, O. Schaetzle, J. M. Paz-García, P. M. Biesheuvel, and C. J. Buisman, "Harvesting Energy from CO 2 Emissions," *Environmental Science and Technology Letters*, vol. 1, no. 1, pp. 31–35, 2013.

[4] R. A. Rica, R. Ziano, D. Salerno, F. Mantegazza, R. van Roij, and D. Brogioli, "Capacitive mixing for harvesting the free energy of solutions at different concentrations," *Entropy*, vol. 15, no. 4, pp. 1388–1407, 2014.

[5] J. Kim, J. Lee, and J. H. Kim, "Overview of pressure-retarded osmosis (PRO) process and hybrid application to sea water reverse osmosis process," *Desalination and Water Treatment*, vol. 43, no. 1-3, pp. 193–200, 2012.

[6] D. A. Vermaas, E. Guler, M. Saakes, and K. Nijmeijer, "Theoretical power density from salinity gradients using reverse electrodialysis," *Energy Procedia*, vol. 20, no. May 2014, pp. 170–184, 2012.

[7] B. B. Sales, M. Saakes, J. W. Post, C. J. Buisman, P. M. Biesheuvel, and H. V. Hamelers, "Direct power production from a water salinity difference in a membrane-modified supercapacitor flow cell," *Environmental Science and Technology*, vol. 44, no. 14, pp. 5661–5665, 2010.

[8] Statkraft, "Is PRO economically feasible? Not according to Statkraft — ForwardOsmosisTech." [Online]. Available: https://www.forwardosmosistech.com/statkraft-discontinues-investments-in-pressure-retarded-osmosis-2/

[9] O. Burheim, B. B. Sales, O. Schaetzle, F. Liu, and H. V. Hamelers, "Auto generative capacitive mixing for power conversion of sea and river water by the use of membranes," *ASME 2011 International Mechanical Engineering Congress and Exposition, IMECE 2011*, vol. 1, no. March, pp. 483–492, 2011.

[10] T. Kim, B. E. Logan, and C. A. Gorski, "A pH-Gradient Flow Cell for Converting Waste CO2 into Electricity," *Environmental Science and Technology Letters*, vol. 4, no. 2, pp. 49–53, 2017.

[11] T. Pandolfo, V. Ruiz, S. Sivakkumar, and J. Nerkar, "General Properties

of Electrochemical Capacitors," *Supercapacitors: Materials, Systems, and Applications*, no. 2013, pp. 69–109, 2013.

[12] R. M. Mayer and I. Duff-Barclay, "Energy Storage Devices Based on Polymers." pp. 197–242, 2017.

[13] D. V. Ragone, "Review of battery systems for electrically powered vehicles," *SAE Technical Papers*, 1968.

[14] C. Zhong, Y. Deng, W. Hu, J. Qiao, L. Zhang, and J. Zhang, "A review of electrolyte materials and compositions for electrochemical supercapacitors," *Chemical Society Reviews*, vol. 44, no. 21, pp. 7484–7539, 2015. [Online]. Available: http://dx.doi.org/10.1039/C5CS00303B

[15] H. Strathmann, *Ion-exchange membrane separation process*, Elsevier, Ed. Elsevier, 2004.

[16] S. Zhang and N. Pan, "Supercapacitors performance evaluation," *Advanced Energy Materials*, vol. 5, no. 6, pp. 1–19, 2015.

[17] Gamry Instruments, "APPLICATION NOTES Testing super-capacitors," *Current*, 1999.

[18] E. P. Randviir and C. E. Banks, "Electrochemical impedance spectroscopy: An overview of bioanalytical applications," *Analytical Methods*, vol. 5, no. 5, pp. 1098–1115, 2013.

[19] Gamry Instruments, "Testing Electrochemical Capacitors Part 2 – Cyclic Charge Discharge and Stacks," *Gamry Application Notes*, no. V, pp. 2–7, 2012. [Online]. Available: https://www.gamry.com/application-notes/

[20] M. Teresa Pérez-Prior, N. Ureña, M. Tannenberg, C. del Río, and B. Levenfeld, "DABCO-functionalized polysulfones as anion-exchange membranes for fuel cell applications: Effect of crosslinking," *Journal of Polymer Science, Part B: Polymer Physics*, vol. 55, no. 17, pp. 1326–1336, 2017.

[21] C. R. Middaugh, E. F. Vanin, and T. H. Ji, "Chemical crosslinking of cell membranes," *Molecular and Cellular Biochemistry*, vol. 50, no. 2, pp. 115–141, 1983.

[22] M. Gil, X. Ji, X. Li, H. Na, J. E. Hampsey, and Y. Lu, "Direct synthesis of sulfonated aromatic poly(ether ether ketone) proton exchange membranes for fuel cell applications," *Journal of Membrane Science*, vol. 234, no. 1-2, pp. 75–81, 2004.

[23] R. S. Yee, K. Zhang, and B. P. Ladewig, "The effects of sulfonated poly(ether ether ketone) ion exchange preparation conditions on membrane properties," *Membranes*, vol. 3, no. 3, pp. 182–195, 2013.

[24] A. Rahimpour, S. S. Madaeni, S. Ghorbani, A. Shockravi, and Y. Mansourpanah, "The influence of sulfonated polyethersulfone (SPES) on surface nano-morphology and performance of polyethersulfone (PES) membrane," *Applied Surface Science*, vol. 256, no. 6, pp. 1825–1831, 2010.

[25] C. Summary, "PubChem CID: 3386966 Structure:," pp. 1–12, 2020.

[26] El-cell Gmbh, “User Manual PAT-Cell Release 2.5,” vol. 3304, no. January, pp. 1–148, 2012.

[27] ——, “User Manual PAT-Core Release 2.21,” pp. 1–23, 2018.

[28] ——, “Product Overview,” 2020.

[29] V. K. Mathur and J. Crawford, “Fundamentals of gas diffusion layers in PEM fuel cells,” *Recent Trends in Fuel Cell Science and Technology*, vol. 400, pp. 116–128, 2007.

[30] K. Scott, *Membrane electrode assemblies for polymer electrolyte membrane fuel cells.* Woodhead Publishing Limited, 2012. [Online]. Available: http://dx.doi.org/10.1016/9780857096371.3.279

Acknowledgments

Tengo a scrivere almeno questa sezione di tesi in Italiano, in modo da riuscire ad esprimermi al meglio. Primi tra tutti volevo ringraziare Andrea, Alessandro e Pietro, innanzitutto per la disponibilità e la pazienza avuta nell’insegnarmi le nozioni base per sopravvivere all’interno di un laboratorio di ricerca (dall’utilizzo degli strumenti fino al ”mai dare da bere ad un acido”) e in secondo luogo per le correzioni e le utilissime revisioni di questo lavoro di tesi.

Ringrazio Jovana, per l’aiuto e il sostegno fornitomi ogni giorno e ancor di più durante il periodo di chiusura dovuto al Covid-19: periodo durante il quale tutti siamo stati costretti a ”navigare a vista”.

Ringrazio tutti i miei amici e le persone care per avermi accompagnato e per aver condiviso con me i preziosi momenti di svago durante tutto il percorso universitario. In particolare desidero ringraziare i RedWine (Francesco, Nicola, Stefano, Riccardo, Veronica e Lorenzo), per i pomeriggi e le sere (e ogni tanto anche le mattine) passate insieme a suonare.

Infine desidero ringraziare la mia famiglia per il supporto morale ed economico al mio percorso di studi e mio fratello Fabio per i preziosi consigli riguardo la scelta della tesi magistrale.